

# UC Santa Barbara

## UC Santa Barbara Previously Published Works

### Title

Quantifying the Electron Donor and Acceptor Abilities of the Ketimide Ligands in  $M(NCtBu_2)_4$  ( $M = V, Nb, Ta$ )

### Permalink

<https://escholarship.org/uc/item/400086tq>

### Journal

Inorganic Chemistry, 54(20)

### ISSN

0020-1669

### Authors

Damon, Peter L  
Liss, Cameron J  
Lewis, Richard A  
[et al.](#)

### Publication Date

2015-10-19

### DOI

10.1021/acs.inorgchem.5b02017

Peer reviewed

# Quantifying the electron donor and acceptor ability of the ketimide ligands in $M(N=C^tBu_2)_4$ ( $M = V, Nb, Ta$ )

*Peter L. Damon,<sup>†</sup> Cameron J. Liss,<sup>‡</sup> Richard A. Lewis,<sup>†</sup> Simona Morochnik,<sup>†</sup> David E. Szpunar,<sup>‡</sup> Joshua Telser,<sup>‡\*</sup> and Trevor W. Hayton<sup>†\*</sup>*

<sup>†</sup>Department of Chemistry and Biochemistry, University of California, Santa Barbara, California 93106, United States

<sup>‡</sup>Department of Biological, Chemical and Physical Sciences, Roosevelt University, 430 S. Michigan Ave. Chicago, Illinois 60605-1394 United States

## ABSTRACT

Addition of 4 equiv of  $\text{Li}(\text{N}=\text{C}^t\text{Bu}_2)$  to  $\text{VCl}_3$  in THF, followed by addition of 0.5 equiv  $\text{I}_2$ , generates the homoleptic V(IV) ketimide complex,  $\text{V}(\text{N}=\text{C}^t\text{Bu}_2)_4$  (**1**), in 42% yield. Similarly, reaction of 4 equiv of  $\text{Li}(\text{N}=\text{C}^t\text{Bu}_2)$  with  $\text{NbCl}_4(\text{THF})_2$  in THF affords the homoleptic Nb(IV) ketimide complex,  $\text{Nb}(\text{N}=\text{C}^t\text{Bu}_2)_4$  (**2**), in 55% yield. Seeking to extend the series to the tantalum congener, a new Ta(IV) starting material,  $\text{TaCl}_4(\text{TMEDA})$  (**3**), was prepared *via* reduction of  $\text{TaCl}_5$  with  $\text{Et}_3\text{SiH}$ , followed by addition of TMEDA. Reaction of **3** with 4 equiv of  $\text{Li}(\text{N}=\text{C}^t\text{Bu}_2)$  in THF results in a isolation of a Ta(V) ketimide complex,  $\text{Ta}(\text{Cl})(\text{N}=\text{C}^t\text{Bu}_2)_4$  (**5**), which can be isolated in 32% yield. Reaction of **5** with  $\text{Tl}(\text{OTf})$  yields  $\text{Ta}(\text{OTf})(\text{N}=\text{C}^t\text{Bu}_2)_4$  (**6**) in 44% yield. Subsequent reduction of **6** with  $\text{Cp}^*_2\text{Co}$  in toluene generates the homoleptic Ta(IV) congener  $\text{Ta}(\text{N}=\text{C}^t\text{Bu}_2)_4$  (**7**), although the yields are poor. All three homoleptic Group 5 ketimide complexes exhibit squashed tetrahedral geometries in the solid state, as determined by X-ray crystallography. This geometry leads to a  $d_{x^2-y^2}^{-1}$  ( ${}^2\text{B}_1$  in  $D_{2d}$ ) ground state, as supported by DFT calculations. EPR spectroscopic analysis of **1** and **2**, performed at X- and Q-band frequencies (~9 and 35 GHz, respectively), further supports the  ${}^2\text{B}_1$  ground state assignment, while comparison of **1**, **2**, and **7** with related Group 5 tetra(aryl), tetra(amido) and tetra(alkoxo) complexes shows a higher M-L covalency in the ketimide-metal interaction. In addition, a ligand field analysis of **1** and **2** demonstrates that the ketimide ligand is both a strong  $\pi$ -donor and strong  $\pi$ -acceptor, an unusual combination found in very few organometallic ligands.

## Introduction

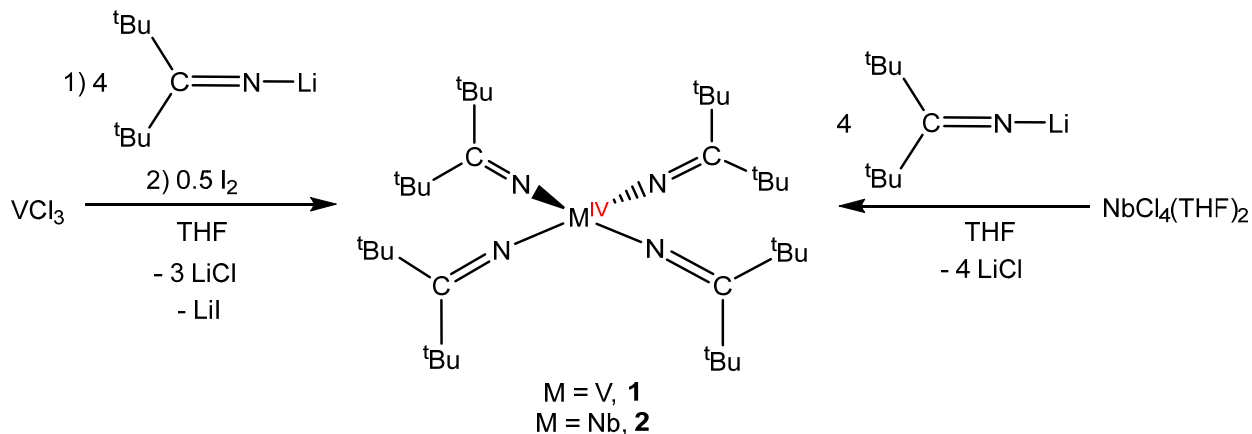
The ketimide ligand,  $[\text{N}=\text{CR}_2]$ , has proven adept at stabilizing high oxidation states, both for transition metal ions and also the actinides.<sup>1-7</sup> For example, in 2010 we reported the synthesis of an isolable Fe(IV) ketimide complex,  $\text{Fe}(\text{N}=\text{C}^t\text{Bu}_2)_4$ ,<sup>3</sup> a rare example of an  $\text{MX}_4$ -type complex of the late first row transition metals.<sup>8</sup> Our group also synthesized the homoleptic Mn(IV) and Co(IV) ketimides,  $\text{M}(\text{N}=\text{C}^t\text{Bu}_2)_4$  ( $\text{M} = \text{Mn}, \text{Co}$ ),<sup>4,6</sup> while Hoffman and co-workers reported the isolation of  $\text{Cr}(\text{N}=\text{C}^t\text{Bu}_2)_4$ .<sup>9</sup> In addition, Kiplinger and co-workers reported the formation of a rare U(V) organometallic,  $\text{Cp}^*_2\text{U}(\text{NDipp})(\text{N}=\text{CPh}_2)$  ( $\text{Dipp} = 2,6\text{-}i\text{Pr}_2\text{C}_6\text{H}_3$ ), stabilized by inclusion of the ketimide ligand.<sup>2</sup> The ability of the ketimide ligand to stabilize high oxidation states likely stems from the orbitals available for the metal-ketimide interaction. DFT calculations on  $\text{Cr}(\text{N}=\text{C}^t\text{Bu}_2)_4$  and  $\text{Co}(\text{N}=\text{C}^t\text{Bu}_2)_4$  reveal that the ketimide ligand is a strong  $\sigma$ - and  $\pi$ -donor, and, as such, should be adept at satisfying the 4+ charge of an M(IV) ion. Interestingly, however, the ketimide ligand also appears to be a good  $\pi$ -acceptor, at least according to DFT calculations.<sup>6,7,9</sup> The unusual combination of  $\pi$ -donor and  $\pi$ -acceptor ability is made possible by the presence of a  $\pi$ -donating nitrogen lone pair and a  $\pi$ -accepting  $\text{C}=\text{N}$  anti-bonding orbital, which is orthogonal to aforementioned nitrogen lone pair. Moreover, an Energy Decomposition Analysis calculation on  $\text{Co}(\text{N}=\text{C}^t\text{Bu}_2)_4$  suggests that the Co-N  $\pi$ -back donation interaction accounts for sizable (ca. 25%) portion of the total Co-N bonding energy in this complex.<sup>6</sup> This finding was somewhat unanticipated, yet it is significant because it suggests that the combined donor/acceptor properties of the ketimide ligand could engender unique structure and reactivity.

To better understand the electronic properties of the ketimide ligand we endeavored to synthesize the tetrakis(ketimide) Group 5 complexes,  $M(N=C^tBu_2)_4$  ( $M = V, Nb, Ta$ ), as the  $d^1$  electronic configuration within these complexes would render them amenable to characterization by a wide variety of spectroscopic techniques, including UV-vis and EPR spectroscopies, which could shed further light on the  $\pi$ -bonding and  $\pi$ -accepting properties of this class of ligand. Herein, we describe the synthesis and comprehensive spectroscopic characterization of  $M(N=C^tBu_2)_4$  ( $M = V, Nb, Ta$ ). Most significantly, this study provides experimental confirmation that the ketimide ligand is, in fact, a good  $\pi$ -acceptor, knowledge that is essential for the further development of the ketimide moiety for use as a co-ligand in metal-centered catalysis. In addition, we describe the synthesis of  $TaCl_4(TMEDA)$ , a potentially useful synthon for Ta(IV) chemistry.

## Results and Discussion

**Synthesis.** Addition of 4 equiv of  $Li(N=C^tBu_2)$  to  $VCl_3$ , in THF, affords a deep green solution. Subsequent addition of 0.5 equiv of  $I_2$  to this solution yields the homoleptic V(IV) ketimide complex,  $V(NC^tBu_2)_4$  (**1**), in moderate yields, after work-up (Scheme 1). Its niobium congener is accessible via a similar metathetical protocol. Thus, addition of 4 equiv of  $Li(N=C^tBu_2)$  to  $NbCl_4(THF)_2$ ,<sup>10</sup> in THF, affords a dark brown solution, which, after work-up, yields the analogous homoleptic Nb(IV) ketimide complex,  $Nb(NC^tBu_2)_4$  (**2**), in moderate yields (Scheme 1). As a solid, complex **1** is dark orange-brown; however, it is dark green in solution. Complex **2** is dark brown, both in the solid state and in solution. Both complexes are very soluble in non-polar solvents, such as hexanes, toluene, and  $Et_2O$ . They are also very soluble in THF, but are insoluble in acetonitrile. Complexes **1** and **2** decompose in the presence of  $CH_2Cl_2$ .

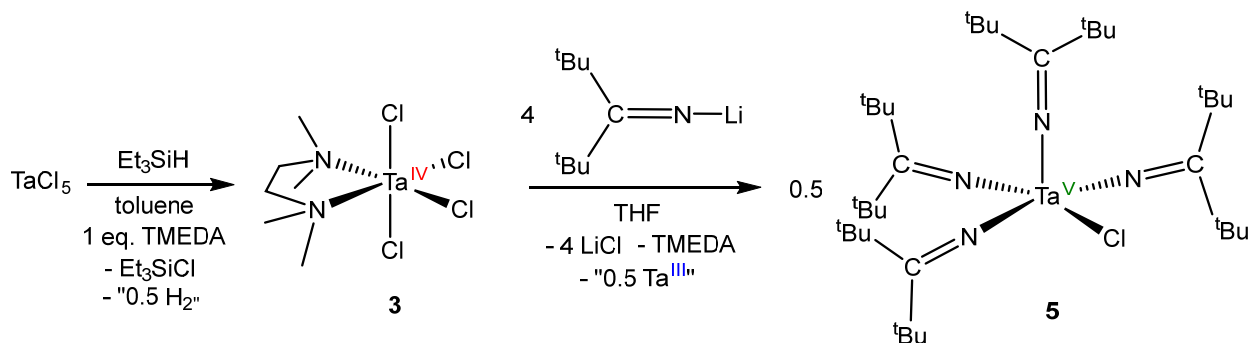
## Scheme 1



The  $^1\text{H}$  NMR spectrum of **1** in  $\text{C}_6\text{D}_6$  exhibits a broad resonance centered at 3.84 ppm (FWHM = 900 Hz), which is assignable to the *tert*-butyl protons of the ketimide ligand. Similarly, the  $^1\text{H}$  NMR spectrum of **2** in  $\text{C}_6\text{D}_6$  exhibits a broad resonance centered at 6.80 ppm (FWHM = 850 Hz), which is assignable to the *tert*-butyl protons of the coordinated ketimide ligand.

Interestingly, unlike previously reported transition metal ketimide complexes from our group,<sup>3,4,6,7</sup> complex **1** is thermally stable: thermolysis of a  $\text{C}_6\text{D}_6$  solution of **1** at 70 °C for 2 h does not result in any signs of decomposition (Figure S2).

## Scheme 2



We next sought to synthesize the tantalum congener to complex **1** and **2**; however, unlike Nb, an easily prepared Ta(IV) starting material has yet to be reported. For example, TaCl<sub>4</sub>(THF)<sub>2</sub> is unknown, and while TaCl<sub>4</sub> is known, its preparation is not straightforward.<sup>11,12</sup> In an effort to synthesize a convenient Ta(IV) synthon we explored the reduction of TaCl<sub>5</sub> with a readily available silane, Et<sub>3</sub>SiH. Reaction of TaCl<sub>5</sub> with 1 equiv of HSiEt<sub>3</sub> in toluene, followed by addition of TMEDA, affords TaCl<sub>4</sub>(TMEDA) (**3**), which can be isolated as an orange crystalline solid in 87% yield after work-up (Scheme 2). The synthesis of **3** mirrors that of TaCl<sub>3</sub> from TaCl<sub>5</sub> and BTCD (BTCD = 3,6-bis(trimethylsilyl)-1,4-cyclohexadiene), which also generates R<sub>3</sub>SiCl as a by-product.<sup>13</sup> Complex **3** is soluble in CH<sub>2</sub>Cl<sub>2</sub>, THF, and acetonitrile, but is insoluble in hexanes and Et<sub>2</sub>O, and only sparingly soluble in toluene. Its <sup>1</sup>H NMR spectrum in CD<sub>2</sub>Cl<sub>2</sub> exhibits two broad singlets, at 2.72 and 8.76 ppm, in a 3:1 ratio. These are assignable to the methyl and methylene resonances of the TMEDA moiety, respectively, and are shifted significantly from those observed for free TMEDA, consistent with coordination of TMEDA to a paramagnetic metal center. Complex **3** was also characterized by X-ray crystallography (See SI for full details). Interestingly, the reduction of TaCl<sub>5</sub> with Et<sub>3</sub>SiH also affords a second, minor product, which can be isolated as a pale blue, CH<sub>2</sub>Cl<sub>2</sub>-insoluble powder in very low yield. This material was subsequently identified as [ {(TMEDA)TaCl<sub>2</sub>(μ-Cl)}<sub>2</sub>][TaCl<sub>6</sub>] (**4**) by X-ray crystallography (see SI for more details).

Addition of 4 equiv of Li(N=C<sup>t</sup>Bu<sub>2</sub>) to **3**, in THF, affords a dark yellow-brown solution. Extraction into hexanes, filtration, and crystallization affords the Ta(V) ketimide, Ta(Cl)(NC<sup>t</sup>Bu<sub>2</sub>)<sub>4</sub> (**5**), as yellow blocks in 32% yield (Scheme 2). The isolation of a Ta(V) product from this reaction suggest that addition of Li(N=C<sup>t</sup>Bu<sub>2</sub>) to **3** results in Ta(IV) disproportionation. However, efforts to identify and isolate the Ta(III) byproduct from the

reaction have proven unsuccessful. The  $^1\text{H}$  NMR spectrum of **5** in  $\text{C}_6\text{D}_6$  exhibits a sharp singlet at 1.36 ppm, assignable to the *tert*-butyl protons of the ketimide ligand. Only one ketimide environment is observed, suggestive of rapid exchange between equatorial and axial ketimide ligand environments about the  $\text{Ta}^{5+}$  center (see below).

Curiously, a direct synthetic route to complex **5** from  $\text{TaCl}_5$  has not been forthcoming. For example, reaction of  $\text{TaCl}_5$  with 4 equiv of  $\text{Li}(\text{N}=\text{C}^t\text{Bu}_2)$ , in THF or DME, results in the formation of complex reaction mixtures, as determined by  $^1\text{H}$  NMR spectroscopy. According to  $^1\text{H}$  NMR spectroscopy, complex **5** is present in the reaction mixture; however, it is but one of many components and it is present only in low yield. To rationalize these results, we note that  $\text{TaX}_5$  ( $\text{X} = \text{Cl}, \text{Br}, \text{I}$ ) readily reacts with a variety of ethereal solvents, including DME and THF, to form alkoxides.<sup>14,15</sup> Thus it seems likely that the *in situ* formation of a tantalum alkoxide during the reaction with  $\text{Li}(\text{N}=\text{C}^t\text{Bu}_2)$  in THF inhibits the desired salt metathesis.

Complex **5** crystallizes in the monoclinic space group  $\text{P}2_1/\text{c}$  with two independent molecules in the asymmetric unit. The solid state molecular structure of one independent molecule is shown in Figure 1. This complex exhibits a distorted square pyramidal structure, as determined by Continuous Shape Measure ( $\text{CSM} = 1.14$ ) developed by Alvarez and co-workers,<sup>16</sup> wherein the chloride ligand and three ketimide ligands occupy the equatorial positions, while one ketimide ligand (N3) occupies the axial position. The Ta-N bond lengths in **5** range from 1.918(4) to 1.990(5) Å, and are similar to those observed in other tantalum ketimides.<sup>17,18</sup> In addition, the average Ta-N-C angle ( $172.7^\circ$ ) is indicative of  $\text{sp}$  hybridization at nitrogen, and is suggestive of significant  $\pi$ -donation from the ketimide to the metal, consistent with our ligand



field analysis (see below).<sup>3,4,6,19</sup> Finally, the Ta-Cl bond lengths (2.498(1), 2.496(1) Å) are similar to those observed for other structurally characterized Ta(V) chlorides.<sup>14,15,20-22</sup>

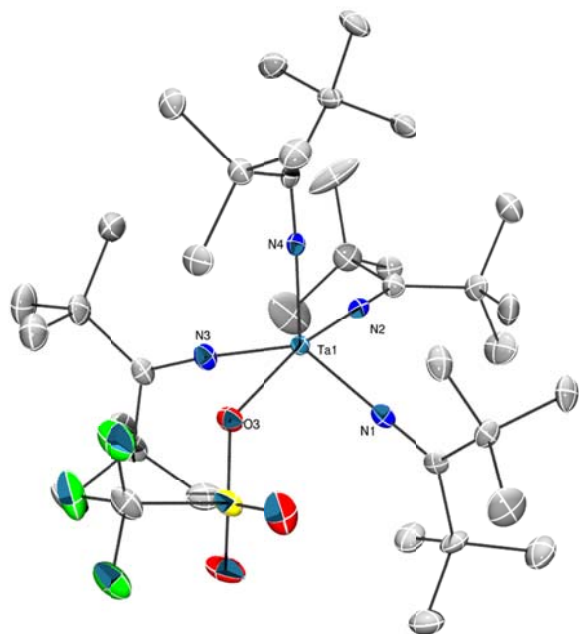
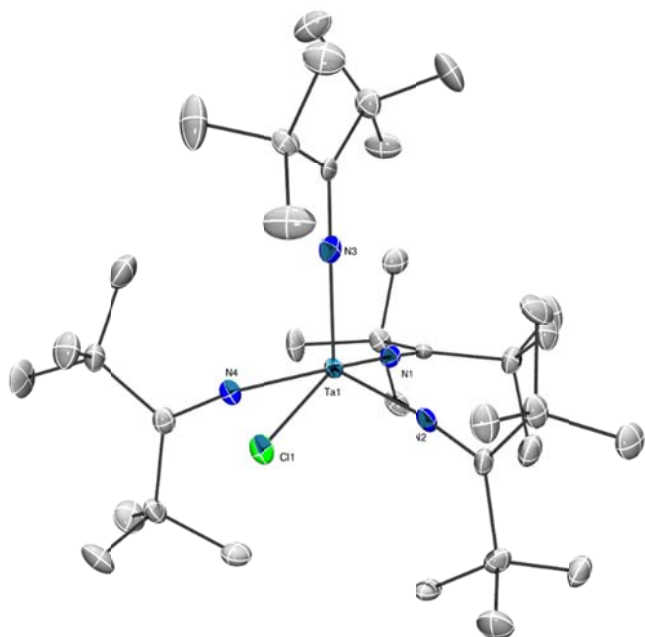
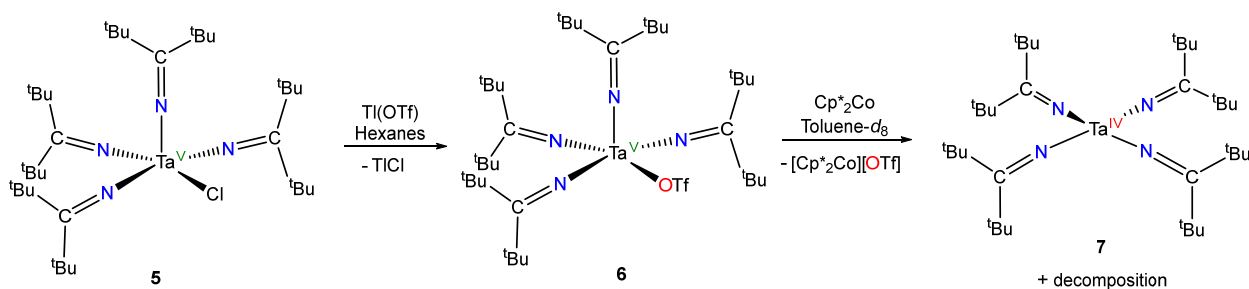


**Figure 1.** Solid state molecular structures of Ta(Cl)(NC<sup>t</sup>Bu<sub>2</sub>)<sub>4</sub> (**5**) (left) and Ta(OTf)(NC<sup>t</sup>Bu<sub>2</sub>)<sub>4</sub> (**6**) (right) with 50% probability ellipsoids. Hydrogen atoms and a second molecule of **5** in the asymmetric unit cell are omitted for clarity. Selected bond distances (Å) and angles (°) for **5**: Ta1-N1 = 1.958(4), Ta1-N2 = 1.967(4), Ta1-N3 = 1.922(4), Ta1-N4 = 1.982(4), Ta1-Cl1 = 2.498(1), N2-Ta1-Cl1 = 79.0(1), N4-Ta1-Cl1 = 79.1(1), N1-Ta1-Cl1 = 156.4(1), N3-Ta1-Cl1 = 103.6(1). Selected bond distances (Å) and angles (°) for **6**: Ta1-N4 = 1.921(2), Ta1-N2 = 1.931(2), Ta1-N1 = 1.955(2), Ta1-N3 = 1.959(3), Ta1-O3 = 2.218(2), N4-Ta1-O3 = 95.27(9), N3-Ta1-O3 = 79.99(9), N1-Ta1-O3 = 80.76(8), N2-Ta1-O3 = 166.11(9).

Complex **5** proved amenable to further synthetic manipulation. For example, reaction of **5** with 1 equiv of Tl(OTf) in hexanes resulted in a color change to deep red. Filtration, followed by crystallization from concentrated hexanes resulted in deposition of Ta(OTf)(N=C<sup>t</sup>Bu<sub>2</sub>)<sub>4</sub> (**6**), as red blocks in 44% yield (Scheme 3). Complex **6** crystallizes in the P2<sub>1</sub>/c space group and, as observed for **5**, it exhibits a distorted square pyramidal geometry about the metal center (Figure 1). Not surprisingly, the metrical parameters of **6** are very similar to those of **5**.

### Scheme 3

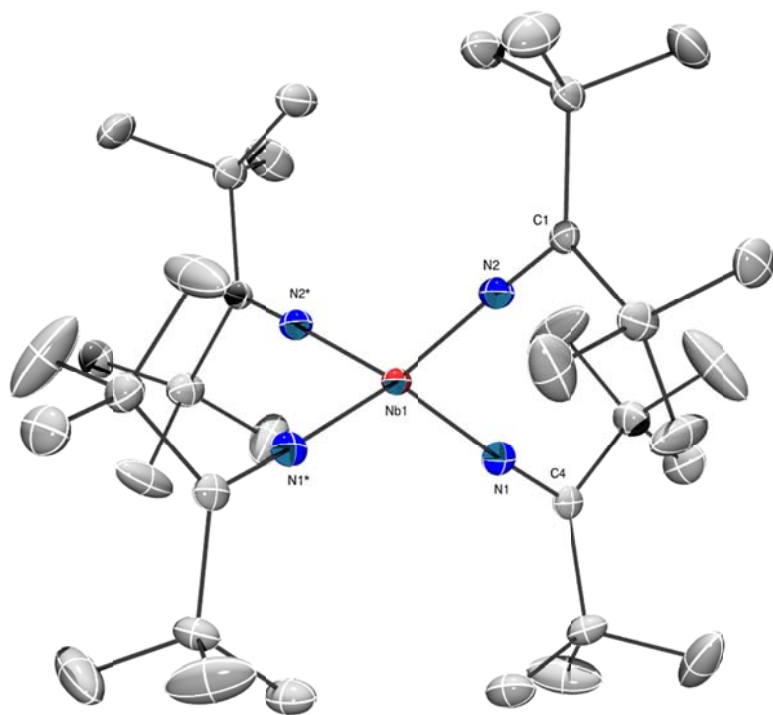
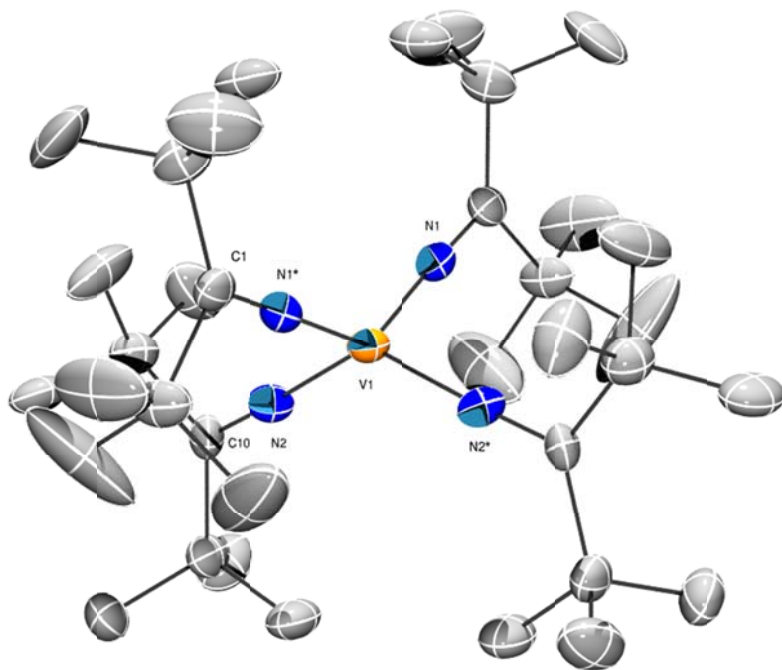


With complexes **5** and **6** in hand, we probed their utility as precursors to the Ta(IV) ketimide complex, Ta(NC<sup>t</sup>Bu<sub>2</sub>)<sub>4</sub> (**7**). However, neither **5** nor **6** proved very amenable to chemical

reduction. For example, reduction of either **5** or **6** with  $\text{KC}_8$  results in the formation of a mixture of products, while reductions with sodium metal or Na/Hg amalgam did not go to completion, even over long reaction times. In contrast, the reaction of **6** with  $\text{Cp}^*_2\text{Co}$  ( $\text{Cp}^* =$  pentamethylcyclopentadienide) appeared to be much more promising. Thus, addition of 1 equiv of  $\text{Cp}^*_2\text{Co}$  to a toluene- $d_8$  solution of **6** results in the formation of a broad singlet at 7.42 ppm (fwhm = 860 Hz) in the  $^1\text{H}$  NMR spectrum, assignable to the *tert*-butyl protons of  $\text{Ta}(\text{NC}^t\text{Bu}_2)_4$  (**7**). Also present in the sample are resonances assignable to  $[\text{Cp}^*_2\text{Co}][\text{OTf}]$ . Unfortunately, most attempts to isolate complex **7** proved unsuccessful, in part because **7** appears to be quite temperature sensitive. However, in a few instances, a few crystals of **7** were isolable, which permitted its characterization by X-ray crystallography (see below).

**X-ray crystallographic analysis of  $\text{M}(\text{NC}^t\text{Bu}_2)_4$  ( $\text{M} = \text{V}, \text{Nb}, \text{Ta}$ ).** Complexes **1**, **2**, and **7** were characterized by X-ray crystallography, and their solid state molecular structures are shown in Figure 2. A selection of relevant metrical parameters can be found in Table 1. In the solid state, **1** crystallizes in the orthorhombic space group *Pnna* and exhibits a squashed tetrahedral geometry about the vanadium center, as evidenced by the two largest N-V-N bond angles ( $\text{N1-V1-N1}^* = 133.1(1)^\circ$  and  $\text{N2-V1-N2}^* = 132.9(1)^\circ$ ). This corresponds to a  $\tau_4$  value of 0.67, where a  $\tau_4$  value of 1 indicates an idealized tetrahedron while a  $\tau_4$  value of 0 indicates an idealized square plane.<sup>23</sup> Complex **1** features V-N bond lengths of 1.837(1) Å and 1.834(1) Å. For comparison, these values are slightly shorter than those of the homoleptic V(IV) amide,  $\text{V}(\text{NMe}_2)_4$ , which displays V-N bond lengths of 1.866(1) to 1.871(1) Å;<sup>24</sup> however, they are within the range exhibited by other V(V) ketimides (1.787 to 1.847 Å).<sup>25-29</sup> For further comparison, the average V-C bond length in  $\text{V}(\text{Mes})_4$  ( $\text{Mes} = 2,4,6\text{-Me}_3\text{C}_6\text{H}_2$ ) is substantially

longer (2.08 Å).<sup>30</sup> Finally, the V-N-C angles (V1-N1-C1= 177.2(1)° and V1-N2-C10 = 176.7(1)°) are suggestive of  $\pi$ -donation to the vanadium center from the ketimide ligand.



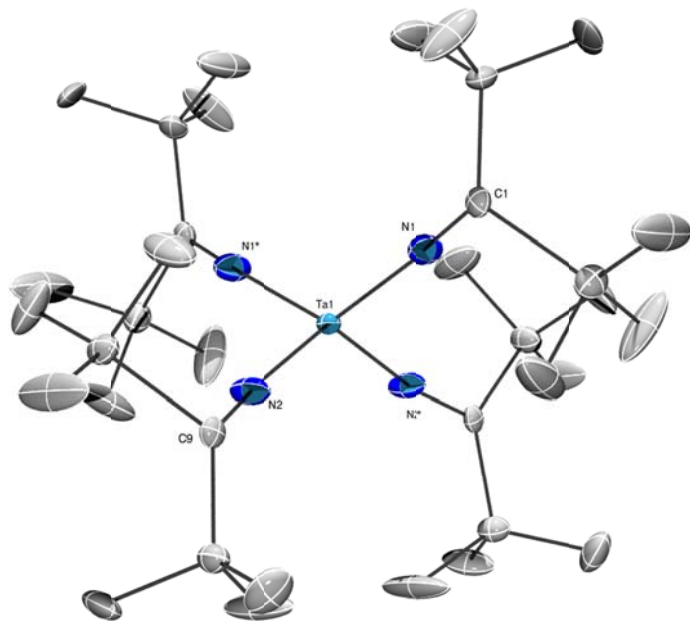


**Figure 2.** Solid state molecular structures of  $\text{V}(\text{NC}^t\text{Bu}_2)_4$  (**1**),  $\text{Nb}(\text{NC}^t\text{Bu}_2)_4$  (**2**), and  $\text{Ta}(\text{NC}^t\text{Bu}_2)_4$  (**7**) with 50% probability ellipsoids. Hydrogen atoms are omitted for clarity. Atoms with an asterisk are generated by symmetry.

Complexes **2** and **7** feature similar squashed tetrahedral geometries in the solid state as that observed for **1**. For example, the largest N-M-N bond angles [**2**:  $\text{N1-Nb1-N1}^* = 129.39(9)^\circ$  and  $\text{N2-Nb1-N2}^* = 129.81(9)^\circ$ ; **7**:  $\text{N1-Ta1-N1}^* = 128.2(1)^\circ$  and  $\text{N2-Ta1-N2}^* = 128.5(1)^\circ$ ] for **2** and **7** correspond to  $\tau_4$  values of 0.72 and 0.73, respectively.<sup>23</sup> As anticipated, the Nb-N bond lengths in **2** ( $\text{Nb1-N1} = 1.937(2)$ ,  $\text{Nb1-N2} = 1.939(2)$  Å) are longer than those observed in **1**, consistent with the presence of the larger  $\text{Nb}^{4+}$  ion, but are shorter than those found in  $\text{Nb}(\text{NPh}_2)_4$  (1.985(3) – 2.029(3) Å).<sup>31</sup> The Ta-N bond lengths in **7** ( $\text{Ta1-N1} = 1.934(2)$ ,  $\text{Ta1-N2} = 1.931(2)$  Å) are identical to those exhibited by **2** and also comparable to those exhibited by complex **5**, despite the difference in oxidation states between the two complexes. For further comparison, these values are comparable to those exhibited by  $\text{MCl}(\text{tmkh})(\text{tBu}_2\text{pz})_2$  ( $\text{M} = \text{Nb}, \text{Ta}$ ;  $\text{tmkh}^{3-} = 2,2,6,6\text{-tetramethyl-5-ketimidohept-3-en-3-imide}$ ;  $\text{tBu}_2\text{pz}^- = 3,5\text{-di-tert-butylpyrazolate}$ ),<sup>32</sup> but

longer than that in Cp\*Ta( $\eta^4$ -C<sub>4</sub>H<sub>6</sub>)( $\kappa^2$ -C,N-C<sub>6</sub>H<sub>4</sub>-2-C(Me)N).<sup>33</sup> Finally, the M-N-C angles in **2** (Nb1-N1-C4 = 176.5(2) and Nb1-N2-C1 = 176.5(2)°) and **7** (Ta1-N1-C1 = 176.3(2) and Ta1-N2-C10 = 174.1(2)°) are indicative of a substantial  $\pi$ -donation from the ketimide to the metal center.

**Table 1.** Comparison of the metrical parameters for M(N=C<sup>t</sup>Bu<sub>2</sub>)<sub>4</sub> (M = Ti, V, Nb, Ta, Cr, Mn, Fe).

| <b>M</b>        | <b>d</b><br><b>count</b> | <b>M-N</b><br><b>distances (Å)</b> | <b>M-N-C</b><br><b>angles (°)</b> | <b>N-M-N</b><br><b>angles (°)<sup>a</sup></b> | $\tau_4^b$ | <b>Ref.</b>   |
|-----------------|--------------------------|------------------------------------|-----------------------------------|---|------------|---------------|
| Ti              | d <sup>0</sup>           | av. 1.87                           | av. 175                           | 114.9<br>111.3                                | 0.96       | <sup>19</sup> |
| V ( <b>1</b> )  | d <sup>1</sup>           | 1.834(1)<br>1.837(1)               | 176.7(1)<br>177.2(1)              | 132.94(9)<br>133.12(9)                        | 0.67       | This work     |
| Nb ( <b>2</b> ) | d <sup>1</sup>           | 1.937(2)<br>1.939(2)               | 176.5(2)<br>176.5(2)              | 129.39(9)<br>129.81(9)                        | 0.72       | This work     |
| Ta ( <b>7</b> ) | d <sup>1</sup>           | 1.931(2)<br>1.934(2)               | 176.3(2)<br>174.1(2)              | 128.4(1)<br>128.2(1)                          | 0.73       | This work     |
| Cr              | d <sup>2</sup>           | 1.784(2)<br>1.785(2)               | 178.4(2)<br>179.1(2)              | 136.1(1)<br>136.2(1)                          | 0.62       | <sup>9</sup>  |
| Mn              | d <sup>3</sup>           | av. 1.79                           | av. 176                           | 151.1(1)<br>150.3(1)                          | 0.42       | <sup>4</sup>  |
| Fe              | d <sup>4</sup>           | 1.771(3)<br>1.775(3)               | 165.5(3)<br>166.6(3)              | 167.1(2)<br>167.6(2)                          | 0.18       | <sup>3</sup>  |
| Co              | d <sup>5</sup>           | av. 1.80                           | av. 167                           | 137.6(2)<br>139.3(2)                          | 0.59       | <sup>6</sup>  |

<sup>a</sup> defined as the two largest N-M-N angles observed in the complex.

<sup>b</sup> as defined in Reference <sup>23</sup>

Complex **1** is the sixth 1<sup>st</sup> row transition metal M(N=C<sup>t</sup>Bu<sub>2</sub>)<sub>4</sub>-type complex to be structurally characterized (Table 1; the present study provides the complete Group 5 series; Hoffman and co-workers have previously reported the complete Group 6 series,<sup>9</sup> these being the only other 2<sup>nd</sup> and 3<sup>rd</sup> row M(N=C<sup>t</sup>Bu<sub>2</sub>)<sub>4</sub> complexes). This series of complexes exhibit an interesting correlation between the coordination geometry about the metal center and the d electron count. Specifically, we observe a gradual planarization of the geometry about the metal ion (as indicated by the  $\tau_4$  value) as the electronic configuration changes from d<sup>0</sup> (Ti) to d<sup>4</sup> (Fe). Previously, we argued that this trend was a consequence of increased crystal field stabilization that would be achieved by flattening to a  $D_{2d}$  structure.<sup>34</sup> Interestingly, the trend reverses at Co ( $\tau_4 = 0.59$ ), which features a d<sup>5</sup> electronic configuration. Presumably, once a d<sup>5</sup> configuration is achieved, at least one d electron must occupy an anti-bonding or partially anti-bonding orbital, which results in a decrease of the crystal field stabilization. This assessment was confirmed by DFT calculations on Co(N=C<sup>t</sup>Bu<sub>2</sub>)<sub>4</sub>, which was found to have a  $d_{x^2-y^2}^2 (d_{xz, yz})^2 d_{z^2}^1$  (<sup>4</sup>A<sub>2</sub> in  $D_{2d}$ ) ground state electronic configuration. These calculations demonstrated that the partially occupied orbitals ( $d_{xz}, d_{yz}, d_{z^2}$ ) all possess considerable  $\pi^*$  Co-N character.<sup>6</sup> Several Group 5 tetra(amido) complexes (e.g., M(NR<sub>2</sub>)<sub>4</sub>) have also been structurally characterized, and a comparison of their metrical parameters with those of **1**, **2**, and **7** is similarly informative. Most interestingly, this class of materials does not exhibit the squashed tetrahedral geometry observed in M(N=C<sup>t</sup>Bu<sub>2</sub>)<sub>4</sub>, and instead exhibit only slightly distorted tetrahedral geometries. For example, the two largest N-V-N inter-ligand angles in V(NMe<sub>2</sub>)<sub>4</sub> are 115.28(6) and 111.42(6)°, substantial smaller than those exhibited by **1**, and close to the 109.5° expected for a perfect tetrahedron.<sup>24</sup> Similarly,

Ta(NPh<sub>2</sub>)<sub>2</sub>(NEt<sub>2</sub>)<sub>2</sub> features a slightly distorted tetrahedral geometry,<sup>35</sup> while Nb(NPh<sub>2</sub>)<sub>4</sub> and Ta(NCy<sub>2</sub>)<sub>2</sub>(NEt<sub>2</sub>)<sub>2</sub> feature some modest flattening, but not at the magnitude observed by complexes **1**, **2**, and **7**. In particular, the two largest N-Nb-N inter-ligand angles for Nb(NPh<sub>2</sub>)<sub>4</sub> are 120.8(1) and 116.7(1)°,<sup>31</sup> and the two largest N-Ta-N inter-ligand angles for Ta(NCy<sub>2</sub>)<sub>2</sub>(NEt<sub>2</sub>)<sub>2</sub> are 123.9(1) and 123.6(1)°. <sup>36</sup> This difference in coordination geometry can be rationalized by arguing that the ketimide ligand is a stronger field ligand than the amide ligand, and the larger CFSE extant in the ketimide complex is enough to overcome the unfavorable steric repulsion engendered by flattening the geometry about the metal center.<sup>35</sup> However, this explanation cannot discriminate between the  $\sigma$ - and  $\pi$ -contributions to the overall ligand field, which differ significantly between amide and ketimide ligands (see below). Thus, to better understand this aspect of metal-ketimide bonding we performed a thorough spectroscopic analysis of complexes **1**, **2**, and **7**.

**EPR Spectroscopy.** The solution phase X-Band EPR spectrum of **1** in hexanes (2 mM) exhibits 8 major features, consistent with a single unpaired electron coupling to the <sup>51</sup>V nucleus ( $I = 7/2$ , ~100%) with  $a(^{51}\text{V}) = 124$  MHz (Figure 3). The large  $a(^{51}\text{V})$  value, along with the  $g$  value ( $g_{\text{iso}} = 1.988 < g_e$ ), are consistent with a predominantly metal centered radical. In addition, hyperfine coupling to the four <sup>14</sup>N nuclei ( $I = 1$ , 100%) of the ketimide ligand is also partly resolved ( $a(^{14}\text{N}) = 10.5$  MHz). The linewidths show a strong dependence on  $|m_I|$ , as has been described in detail for [VO(acac)<sub>2</sub>],<sup>37</sup> and was also seen in several V(IV) phosphine complexes.<sup>38</sup> For comparison with other oganovanadium(IV) complexes, Cp<sub>2</sub>V(SPh)<sub>2</sub> and Cp<sub>2</sub>V(S<sub>5</sub>) exhibit nearly identical isotropic  $g$  and  $a(^{51}\text{V})$  values as those exhibited by complex **1**.<sup>39,40</sup> Also relevant are the homoleptic V(IV) complexes that feature tetra(aryl), tetra(amido), and tetra(alkoxido) ligand sets.<sup>41-44</sup> One of the tetra(aryl) complexes was observed only *in situ* by Alonso et al.,<sup>41</sup> but



another,  $V(\text{Mes})_4$ , was studied not only in fluid solution, but as a doped single crystal (diamagnetic  $Ti(\text{Mes})_4$  host),<sup>42</sup> affording likely the most accurate and complete spin Hamiltonian parameters for any complex relevant to the present work. The EPR investigations and analysis of the tetra(amido)<sup>43</sup> and tetra(alkoxido)<sup>44</sup> complexes were also very thorough, with a variety of solvents and diamagnetic hosts (the  $Ti(\text{IV})$  congeners) employed. These and other EPR parameters of interest are summarized in Table 2.

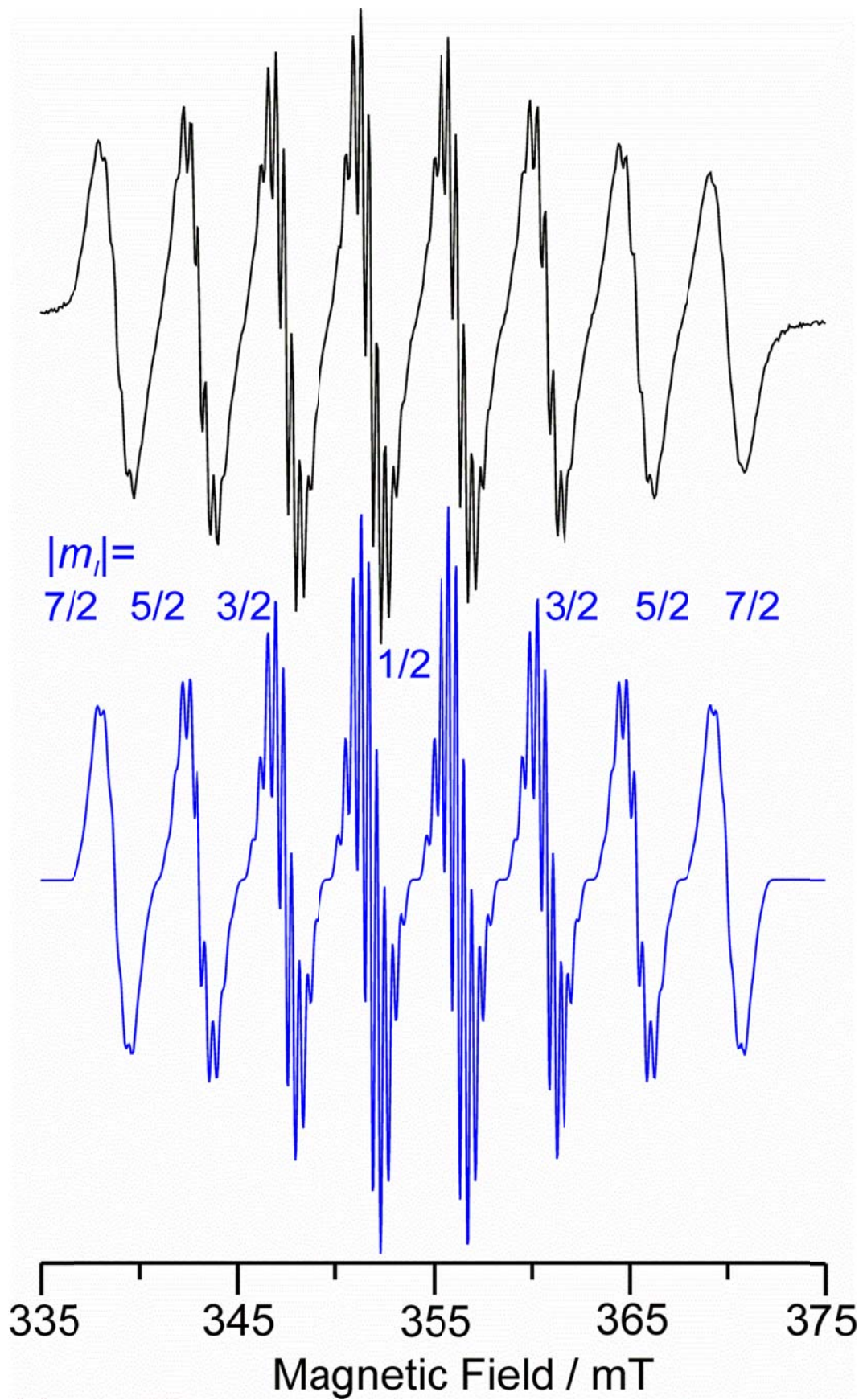


**Figure 3.** Room temperature X-Band EPR spectrum of **1** (2 mM in hexanes). Simulated spectrum shown in blue. Experimental conditions: microwave frequency = 9.856 GHz, microwave power = 1.0 mW, field modulation = 1.0 G, time constant = 0.32 ms, average of 3 250-s scans. Simulation parameters:  $g = 1.9885$ ,  $a(^{51}\text{V}) = 124$  MHz,  $a(^{14}\text{N})_4 = 10.5$  MHz, Gaussian line width = 5 MHz, to match the resolved splitting in the center of the spectrum (an expansion of this central region is shown in Figure S20, Supporting Information). The increased line broadening that occurs with higher magnitude  $^{51}\text{V}$   $m_I$  transitions (e.g.,  $\langle m_S, m_I | = \langle -1/2, \pm 7/2 | \rightarrow \langle +1/2, \pm 7/2 |$ ; see  $|m_I|$  labels on simulated trace; absolute values are given because the sign of  $a_{\text{iso}}$  is unknown from experiment) is reproduced using the model of Froncisz and Hyde,<sup>45</sup> with their  $A$ -strain factor,  $c_1$  (here isotropic) = 1.5 MHz. When the ligand hyperfine coupling was not resolved, it was possible to match all transitions even more exactly (see Figure S19, Supporting Information).

**Table 2.** Spin Hamiltonian parameters for Group 5 complexes relevant to this study.

| Complex  | $g_{\text{iso}}$<br>(fluid solution) | $g_{\text{avg}}$<br>(frozen solution) | $g_{\parallel}, g_{\perp}$<br>(frozen solution) | $a_{\text{iso}}$<br>(fluid solution, MHz) | $A_{\text{avg}}$<br>(frozen solution, MHz) | $A_{\parallel}, A_{\perp}$<br>(frozen solution, MHz) | Ref.          |
|--|--------------------------------------|---------------------------------------|---|---|--|--|---------------|
| $[\text{V}(\text{N}=\text{C}^t\text{Bu}_2)_4]$ , <b>1</b> <sup>a</sup>   | 1.9885(5)                            | 1.983                                 | 1.979(1),<br>1.985(5)                           | 124(2)                                    | 125  | 245(5),<br>65(15)                                    | This work     |
| $[\text{Nb}(\text{N}=\text{C}^t\text{Bu}_2)_4]$ , <b>2</b>   | 1.9840(5)                            | 1.988                                 | 1.966<br>(2),<br>1.999(5)<br><sup>b</sup>       | 185(5)                                    | 150  | 300(10),<br>80(20) <sup>b</sup>                      | This work     |
| $[\text{Ta}(\text{N}=\text{C}^t\text{Bu}_2)_4]$ , <b>7</b>   | 1.955(5)                             | 1.979                                 | 1.998,<br>1.970 <sup>c</sup>                    | 250(10)                                   | 250  | 335,<br>210  | This work     |
| $[\text{V}(\text{C}_6\text{Cl}_5)_4]$  | 1.965                                | ---                                   | 1.925,<br>[1.985] <sup>d</sup>                  | 185                                       | ---  | 385,<br>[85] <sup>e</sup>                            | <sup>41</sup> |
| $[\text{Nb}(\text{C}_6\text{Cl}_5)_4]$   | ---                                  | 1.940                                 | 1.883,<br>1.969                                 | ---                                       | 371  | 598,<br>258  | <sup>46</sup> |
| $\text{V}(\text{Mes})_4$ <sup>f</sup>  | 1.972                                | 1.968                                 | 1.925,<br>1.989                                 | 172.4                                     | 189.8                                      | 370.5,<br>99.5                                       | <sup>42</sup> |
| $\text{V}(\text{N}(\text{C}_6\text{H}_4\text{-}2\text{-}^t\text{Bu}))(\text{NHMe}_2)_2\text{Cl}_2$<br><sup>g</sup> | 1.973                                | 1.973                                 | 1.948,<br>1.986                                 | 260                                       | 260  | 458,<br>158  | <sup>47</sup> |
| $\text{V}(\text{NEt}_2)_4$   | 1.976                                | 1.976                                 | 1.957,<br>1.985                                 | 180                                       | 180  | 372,<br>84   | <sup>43</sup> |
| $\text{V}(\text{O}^t\text{Bu})_4$  | 1.964(5)                             | 1.969(5)                              | 1.940(5),<br>1.984(5)                           | 192(6)                                    | 197(15)                                    | 375(15),<br>108(12)                                  | <sup>44</sup> |
| $\text{Cp}_2\text{V}(\text{SPh})_2$  | 2.00                                 | -                                     | -   | 175                                       | -  | -  | <sup>40</sup> |
| $\text{VCl}_4(\text{PET}_3)_2$   | 1.981                                |                                       | 1.972,<br>1.985                                 | 252                                       |  | 450,<br>147  | <sup>38</sup> |
| $\text{NbCl}_4(\text{PET}_3)_2$  | 1.927                                |                                       | 1.959,  | 381                                       |  | 599,   | <sup>38</sup> |

|  |                  |       |                 |         |     |             |                  |
|--|------------------|-------|-----------------|---------|-----|-------------|------------------|
|  |                  |       | 1.912           |         |     | 276         |                  |
| TaCl <sub>4</sub> (PEt <sub>3</sub> ) <sub>2</sub>                     | 1.740            |       | 1.831,<br>1.695 | 514     |     | 730,<br>413 | <sup>38</sup>    |
| [(MeCp)Nb(C <sub>7</sub> H <sub>7</sub> )] <sup>h</sup>                | 1.986            | -     | -               | 94.5    | -   | -           | <sup>48</sup>    |
| [CpTa(C <sub>7</sub> H <sub>7</sub> )] <sup>h</sup>                    | 1.944            | 1.944 | 1.989,<br>1.921 | 171     | 157 | 428, 22     | <sup>49</sup>    |
| [(MeCp)Ta(C <sub>7</sub> H <sub>7</sub> )] <sub>h</sub>                | 1.945            | 1.943 | 1.987,<br>1.921 | 199     | 192 | 465, 56     | <sup>49</sup>    |
| [Cp*Ta(C <sub>7</sub> H <sub>7</sub> )] <sup>h</sup>                   | 1.949            | 1.948 | 1.989,<br>1.927 | 316     | 306 | 582,<br>168 | <sup>49</sup>    |
| [ <sup>X,R</sup> <sub>i</sub> [NNN <sup>sq*</sup> ]TaCl <sub>3</sub> ] | 1.958 –<br>1.964 | ---   | ---             | 81 – 92 | --- | ---         | <sup>50,51</sup> |

<sup>a</sup> These parameters are based on X-band spectra. Frozen solution Q-band spectra gave:  $g_{\parallel} = 1.979$ ,  $g_{\perp} = 1.987$ ,  $A_{\parallel}(^{51}\text{V}) = 250$  MHz,  $A_{\perp}(^{51}\text{V}) = 65$  MHz.

<sup>b</sup> These parameters are for the majority species. The frozen solution spectrum of **2** is very sensitive to freezing artifacts. Frozen solution Q-band spectra gave:  $g_{\parallel} = 1.979$ ,  $g_{\perp} = 1.995$ ,  $A_{\parallel}(^{93}\text{Nb}) = 310$  MHz,  $A_{\perp}(^{93}\text{Nb}) = 80$  MHz. However, species with  $A_{\parallel} = 365$  MHz were also observed at X-band under slower freezing conditions, which give  $A_{\text{avg}} = 175$  MHz – much closer to the fluid solution value.

<sup>c</sup> These parameters roughly reproduce one species found in frozen solution. No error ranges are given because of the approximate nature of this simulation and the lack of corroborating 35 GHz EPR data, in contrast to **1** and **2**.

<sup>d</sup> Not reported, but calculated here using the reported  $g_{\text{iso}}$  and  $g_{\parallel}$  values.

<sup>e</sup> Not reported, but calculated here using the reported  $a_{\text{iso}}$  and  $A_{\parallel}$  values.

<sup>f</sup> In addition to a fluid solution of V(Mes)<sub>4</sub> (Mes = 2,4,6-Me<sub>3</sub>C<sub>6</sub>H<sub>2</sub>), a single crystal of Ti(Mes)<sub>4</sub> doped with V(Mes)<sub>4</sub> was studied, so that the full **g** and <sup>51</sup>V hyperfine coupling tensors were determined with high precision:  $g_x = 1.984$ ,  $g_y = 1.994$ ,  $g_z = 1.925$ ;  $A_x = 80.6$ ,  $A_y = 118.4$ ,  $A_z = 370.5$  MHz; these are converted to axial tensors for easier comparison with the other entries.

<sup>g</sup> This is but one of a large number of five- and six-coordinate V(IV) complexes reported in this paper; that presented here is more relevant to the ketimides. It is representative of a series of five-coordinate V(IV) imido complexes, V(=NR)(NHMe<sub>2</sub>)<sub>2</sub>Cl<sub>2</sub> where R = five different bulky aryl or alkyl substituents. Their EPR parameters vary minimally as a function of R group as seen in Table 5 of Bigmore *et al.*<sup>47</sup> Their A values have been converted from G to MHz using their reported g values.

<sup>h</sup> These are considered as Nb(IV) or Ta(IV) complexes by virtue of the cycloheptatrienyl ligand being counted as a trianion (10  $\pi$  electrons, Hückel aromatic), along with the cyclopentadienyl monoanion.

<sup>i</sup> The <sup>X,R</sup>[NNN<sup>sq\*</sup>]<sup>2-</sup> ligand is the semiquinone form of <sup>X,R</sup>[NNN<sup>cat</sup>]<sup>3-</sup>, where, e.g., <sup>OMe,iPr</sup>[NNN<sup>cat</sup>]<sup>3-</sup> is the trianion of bis(2-isopropylamino-4-methoxyphenyl)amine (X = 4-OMe; F, H, Me, and <sup>t</sup>Bu; R = 2-<sup>i</sup>Pr; 3,5-C<sub>6</sub>H<sub>3</sub>Me<sub>2</sub>). These complexes are neither truly Ta(V) nor Ta(IV) as a result of the non-innocent ligand. Simulations of room temperature spectra of four complexes were presented, but no parameters were given; the range of  $g_{\text{iso}}$  and  $a_{\text{iso}}$  values presented here are taken from legends to a composite figure in Supporting Information.<sup>50</sup>

The room temperature EPR spectrum of **2** in hexanes (2 mM) consists of a 10 line pattern, consistent with a single unpaired electron coupling to one  $^{93}\text{Nb}$  center ( $I = 9/2$ , 100%) with  $a_{\text{Nb}} = 184$  MHz (Figure 4). Hyperfine coupling to  $^{14}\text{N}$  was not resolved in this spectrum. Again, the  $g$  value falls within the range of a transition metal centered radical ( $g_{\text{iso}} = 1.984$ ). Most relevant is the structurally characterized (in contrast to its V congener) homoleptic tetra(aryl) Nb(IV) complex,  $[\text{Nb}(\text{C}_6\text{Cl}_5)_4]$ .<sup>46</sup> The spin Hamiltonian parameters for this complex are given in Table 2 and show that the  $^{93}\text{Nb}$  hyperfine coupling constant in  $[\text{Nb}(\text{C}_6\text{Cl}_5)_4]$  is much larger than in **2**. This difference, which is also seen for the V complexes, can be qualitatively explained by the greater covalency (via  $\sigma$ - and  $\pi$ -bonding; see below) in **2**, as opposed to the more ionic  $\sigma$ -only bonding in the pentachlorophenyl complex.

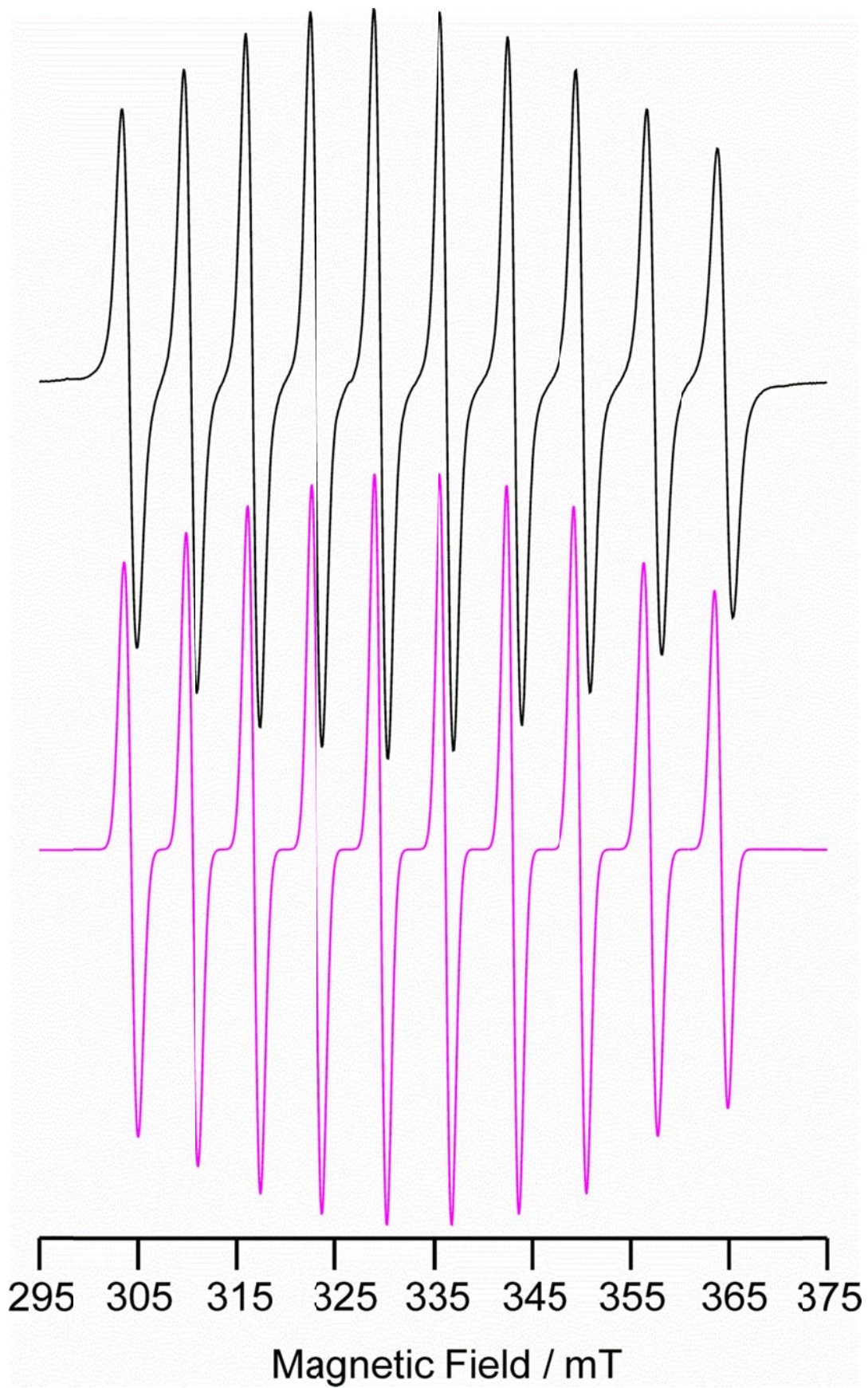


**Figure 4.** Room temperature X-Band EPR spectrum of **2** (2 mM in hexanes). Experimental conditions: microwave frequency = 9.290 GHz, microwave power = 1.0 mW, field modulation = 0.2 G, time constant = 20 ms, average of 25 20-s scans. Simulation parameters:  $g = 1.9840$ ,  $a(^{93}\text{Nb}) = 185$  MHz, Gaussian line width = 20 MHz, to match the central transitions. The increased line broadening that occurs with higher magnitude  $^{93}\text{Nb}$   $m_I$  transitions is reproduced using the model of Froncisz and Hyde,<sup>45</sup> with their  $A$ -strain factor,  $c_1$  (here isotropic) = 2.5 MHz.

The solution phase EPR spectrum of **7**, generated in situ in toluene- $d_8$  by reaction of **6** with 1 equiv of  $\text{Cp}^*_2\text{Co}$ , exhibits the expected 8 line signal, consistent with a single unpaired electron coupling to  $^{181}\text{Ta}$  ( $I = 7/2$ , 100%). In the spectrum shown in Figure 5, complex **7** exhibits a hint of resolved hyperfine coupling to the  $^{14}\text{N}$  nuclei of the ketimide ligand. As shown on an expanded field scale in Figure S20 (Supporting Information), we estimate this coupling at  $a(^{14}\text{N}) \approx 30$  MHz. For comparison, the corresponding well resolved central signals for **1** are also shown in Figure S20, demonstrating the good fit to that region ( $|m_I| = 1/2$ ), which is unaffected by hyperfine dependent line broadening effects. The observed  $g_{\text{iso}}$  value ( $g_{\text{iso}} = 1.955$ ) again falls in the range of transition metal centered radicals and the  $a_{\text{iso}}$  value ( $a_{\text{iso}} = 250$  MHz) continues the trend of increasing  $a_{\text{iso}}$  values of the Group 5 ketimides on going down the column, despite the decrease in  $g_N$  from V to Nb to Ta. A similar trend was seen in the  $\text{MCl}_4(\text{PEt}_3)_2$  ( $M = \text{V}, \text{Nb}, \text{Ta}$ ) series, in which the  $a_{\text{iso}}$  values increased from 252 to 381 to 514 MHz on going down the group.<sup>38</sup> As seen in Table 2, the  $^{181}\text{Ta}$  hyperfine coupling is also in the range reported for the hydrocarbyl complexes,  $(\text{CpR})\text{Ta}(\text{C}_7\text{H}_7)$  ( $R = \text{H}, \text{Me}, \text{Me}_5$ ),<sup>49</sup> and is much larger than that reported for a series of tantalum complexes with a non-innocent pincer ligand.<sup>51</sup>

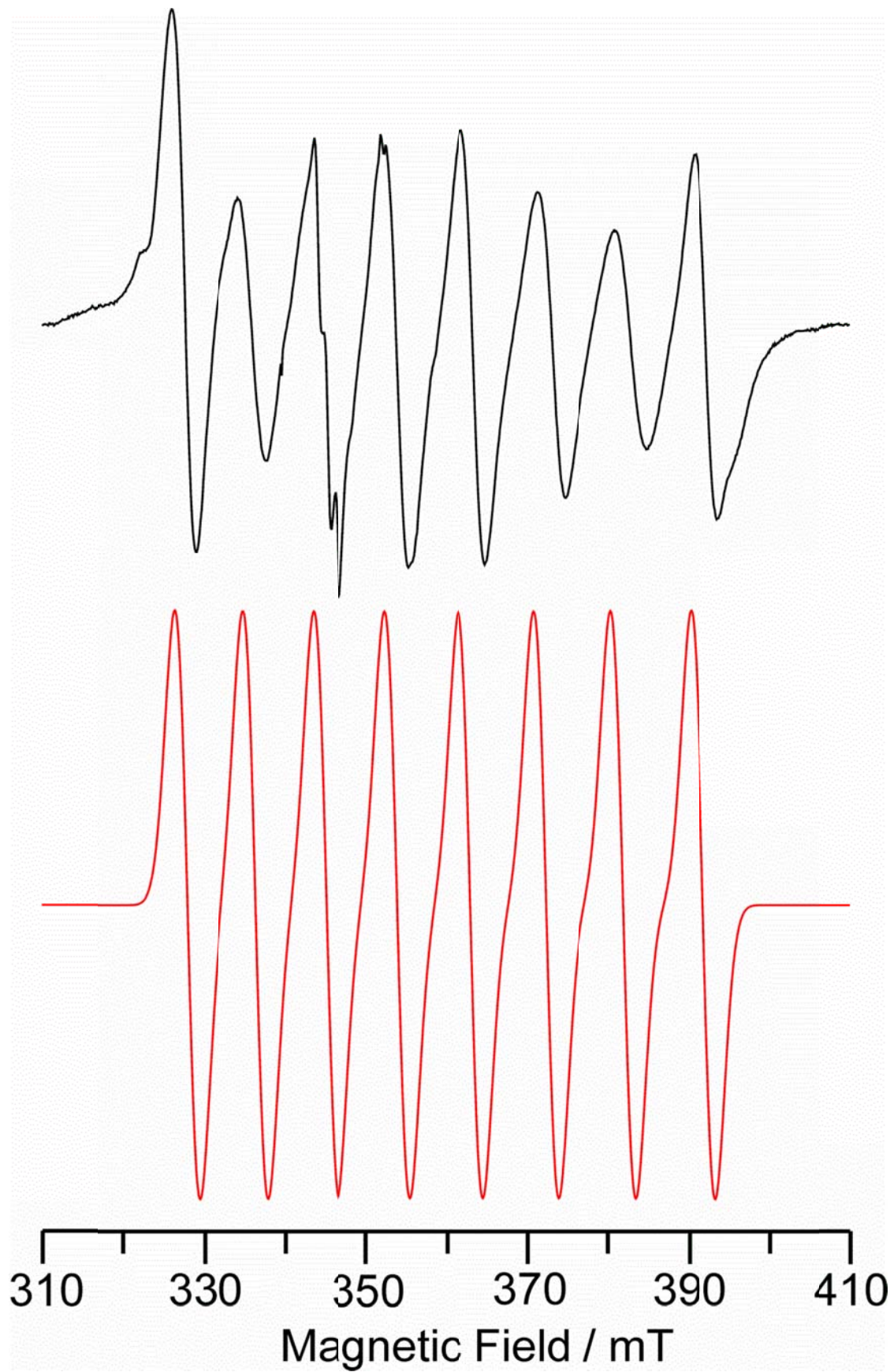




**Figure 5.** Room temperature X-Band EPR spectrum of **7** (0.02 mM in toluene- $d_8$ ). Experimental conditions: microwave frequency = 9.858 GHz, microwave power = 1.0 mW, field modulation = 1.0 G, time constant = 10 ms, average of 20 10-s scans. Simulation parameters:  $g = 1.955$ ,  $a(^{181}\text{Ta}) = 250$  MHz, Gaussian line width = 50 MHz. No attempt was made to model any A strain effects, in contrast to the situation for **1** (Fig. 3) and **2** (Fig. 4), but the  $^{14}\text{N}$  hyperfine coupling is shown on an expanded scale in Figure S20 (Supporting Information).

Being the most stable of the three, the frozen solution EPR spectra of **1** were investigated under a variety of experimental conditions. As shown in Figure 6, in hexanes at 125 K, complex **1** displays average  $g$  and  $A$  values in good agreement with the room temperature isotropic (i.e., rotationally averaged) values (see Table 2), but with significant uniaxial anisotropy, defined here as the  $z$ -direction ( $A_x = A_y = A_{\perp} = 65$  MHz,  $A_z = A_{\parallel} = 245$  MHz). Similar EPR anisotropy has been observed in the pseudo four-coordinate V(IV) complex  $[\text{Cp}_2\text{V}(\text{dbm})][\text{ClO}_4]$  (dbm = dibenzoylmethanate)<sup>52</sup> and in  $\text{V}(\text{Mes})_4$ .<sup>42</sup> Indeed, the ratio of  $A_{\parallel}/A_{\perp}$  in  $\text{V}(\text{Mes})_4$  equals 3.72, and in **1** this ratio is 3.77. The origin of this anisotropy will be discussed below. The X-band EPR spectrum of **1** recorded in toluene solution at 20 K (Figure S21, Supporting Information) was similar, but not identical to that shown here. This may be a consequence of the tetrakis(ketimide) complexes being rather flexible, as next shown more convincingly for the Nb congener.

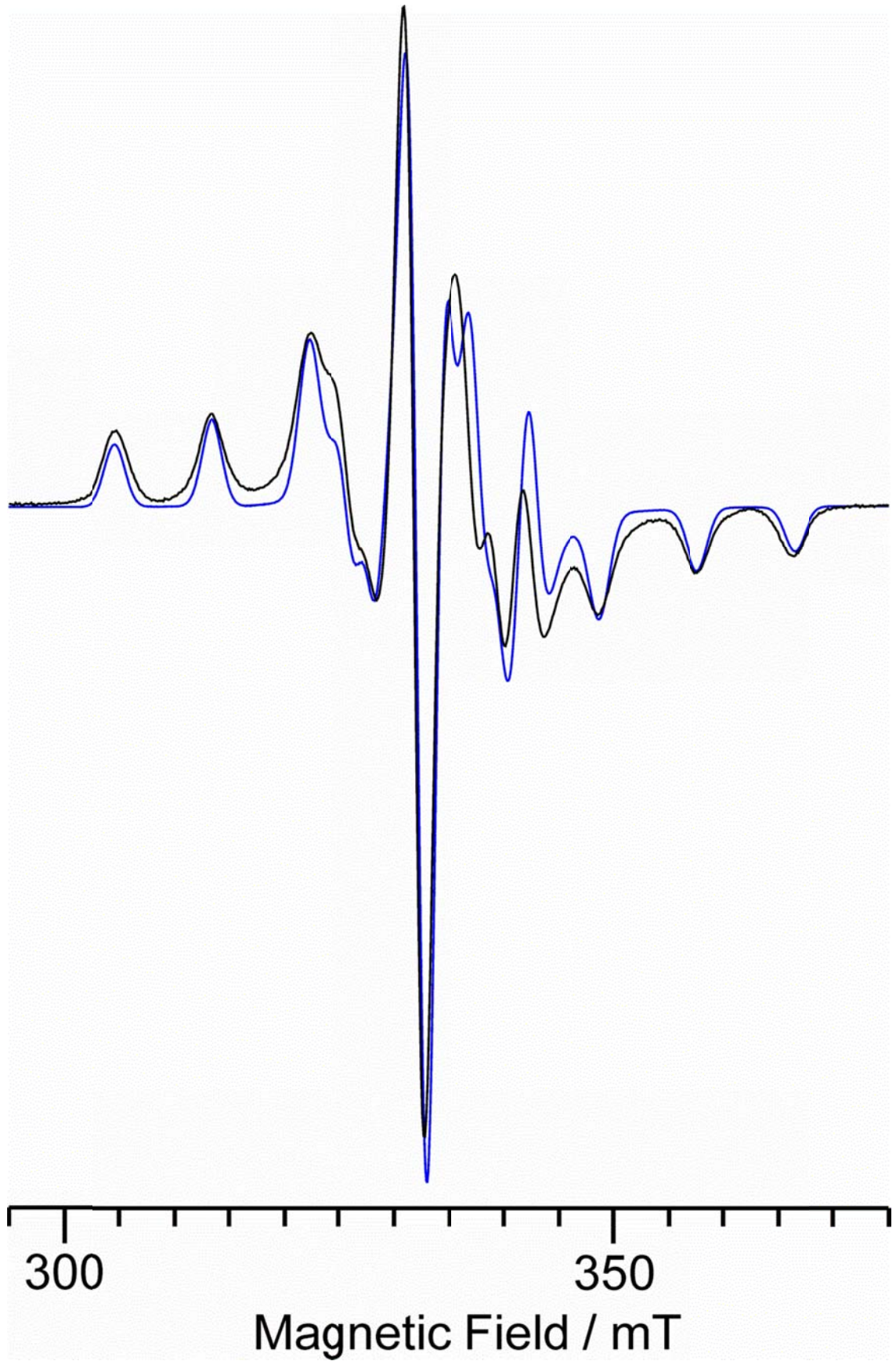


**Figure 6.** Frozen-solution X-Band EPR spectrum (black = experimental, red = simulated) of **1** (2 mM in hexanes) at 125 K. Experimental conditions: microwave frequency = 9.296 GHz, microwave power = 2.0 mW, modulation = 0.5 G, time constant = 2.56 ms, average of 33 20-s scans. Simulation parameters:  $g = [1.985, 1.985, 1.979]$ ,  $A(^{51}\text{V}) = [65, 65, 245]$  MHz, Gaussian line widths = 30 MHz.

We also recorded the 35 GHz (“Q”-band) EPR spectrum of **1** at 2 K in toluene (Figure 7). Under these experimental conditions, the spectra are in “rapid passage” mode and appear as the absorption lineshape.<sup>53</sup> This presentation mode is helpful for observing broad features, but is less so for the relatively narrow lines of **1**. Nevertheless, the use of a second EPR resonant frequency is very helpful in showing the validity of a set of simulation parameters as the  $g$  values are field dependent, while the hyperfine couplings are not. As can be seen from the figure caption, the simulation parameters are essentially unchanged from those determined from X-band spectra (which were, in addition, recorded at higher temperature and under “slow passage”, i.e., “normal” conditions). The increase in frequency to 35 GHz, however, is not sufficient to separate the parallel from the perpendicular transitions. To achieve this, as has been shown in vanadyl complexes, microwave frequencies at 95 GHz (W-band)<sup>54</sup> or higher<sup>55</sup> would be needed.

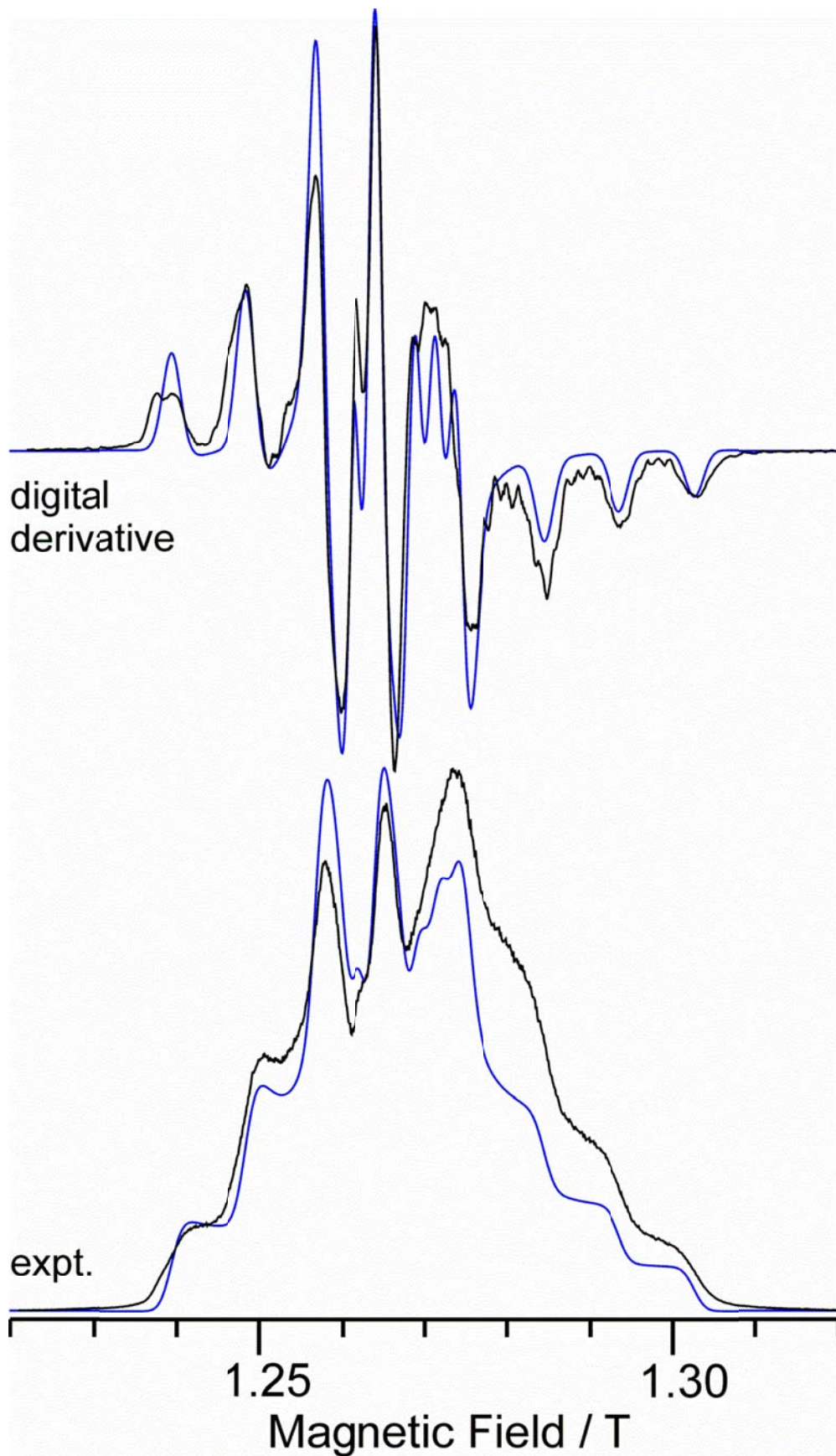


**Figure 7.** Low temperature (2 K) Q-Band EPR spectrum of **1** (0.1 mM in toluene). The lower pair of traces are the experimental spectrum (black trace), together with a simulation (blue trace), while the upper pair is a digital derivative with a simulation. Experimental conditions: microwave frequency = 35.2076 GHz, microwave power = 2 mW, field modulation = 1.0 G, time constant = 16 ms, single 120 s scan. Simulation parameters:  $\mathbf{g} = [1.987, 1.987, 1.979]$ ,  $\mathbf{A}({}^{51}\text{V}) = [65, 65, 250]$  MHz,  $W = 30, 30, 35$  MHz.

ENDOR spectroscopy of V(IV) complexes is rather limited, and has been chiefly performed on vanadyl complexes, such as in pioneering work by van Willigen and co-workers,<sup>56,57</sup> and more recently by Britt and co-workers,<sup>58,59</sup> and by others.<sup>60,61</sup> We therefore recorded 35 GHz CW ENDOR spectra of complex **1**, partly to test the feasibility of ENDOR on such a system. We indeed readily observed  ${}^1\text{H}$ ,  ${}^{14}\text{N}$ , and  ${}^{51}\text{V}$  ENDOR from this complex, as shown in Figure S23. The  ${}^1\text{H}$  ENDOR signals are centered at the proton Larmor frequency ( $\sim 53$  MHz) and show very small hyperfine coupling, as expected for the *tert*-butyl hydrogen atoms, which are relatively distant from the paramagnetic metal center. The  ${}^{51}\text{V}$  ENDOR signals are of qualitative interest only, but are consistent with  $A_{\parallel} = 240$  MHz (i.e., features centered at  $A_{\parallel}/2 = 120$  MHz). The  ${}^{14}\text{N}$  signals also confirm the results of EPR spectroscopy. Absent a complete ENDOR study, it is not appropriate to make a definitive correspondence between the  ${}^{14}\text{N}$  hyperfine splitting observed by EPR and that by  ${}^{14}\text{N}$  ENDOR. This is because one is comparing fluid solution X-band EPR spectra, which provide  $a_{\text{iso}}({}^{14}\text{N})$  (i.e., an average coupling value of all molecular orientations) to frozen solution Q-band ENDOR spectra, recorded only at  $g_{\parallel}$  which thus provide only  $A_{\parallel}({}^{14}\text{N})$  (i.e., the coupling along the parallel ( $z$ ) direction assuming co-linearity of  $\mathbf{A}$  and  $\mathbf{g}$ ). Nevertheless,  $A_{\parallel}({}^{14}\text{N}) \approx 14$  MHz is consistent with  $a_{\text{iso}}({}^{14}\text{N}) = 10.5$  MHz, and also with DFT calculations described below.

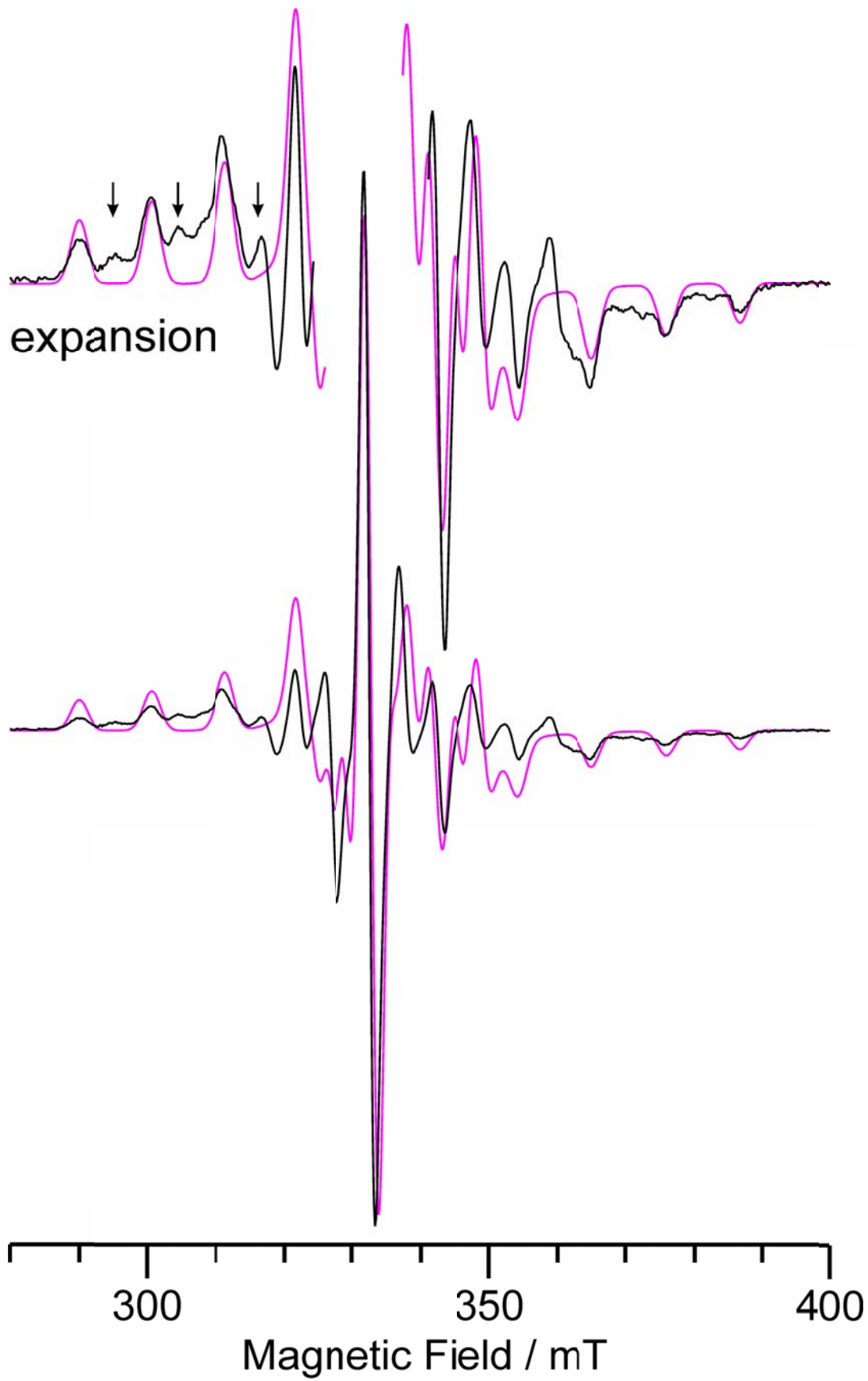


**Figure 8.** Frozen-solution X-Band EPR spectrum of **2** (2 mM in toluene) at 20 K. Several  $A_{\parallel}$  features of a second species are indicated by arrows in the upper, expanded vertical scale spectra; no attempt was made to simulate or quantify this minor species. Experimental conditions: microwave frequency = 9.373 GHz, microwave power = 2 mW, field modulation = 15 G, time constant = 160 ms, single 90 s scan. Simulation parameters (magenta traces):  $g = [1.999, 1.999, 1.966]$ ,  $A(^{93}\text{Nb}) = [80, 80, 300]$  MHz, Gaussian line widths = 35 MHz.

Frozen solution EPR spectra of complex **2** proved more difficult to obtain as a homogeneous species, despite multiple attempts. A representative spectrum, recorded at 20 K in toluene solution, is shown in Figure 8. This spectrum clearly reveals that there are two species present in the sample, which have similar EPR signatures, suggesting that they are only slightly different structurally. Only one species is present in fluid solution (Figure 4), albeit with no resolution of ligand hyperfine, which suggests that these two species can interconvert at room temperature. We made several attempts to generate a homogenous sample by freezing the solution as quickly as possible, however this did not completely mitigate the heterogeneity. Nonetheless, the majority species gives average  $g$  and  $A$  values in reasonable agreement with the room temperature isotropic values (see Table 2). The 35 GHz 2 K spectrum of **2** proved slightly more homogeneous (Figure 9), which may be a function of the smaller sized EPR tubes, allowing for faster freezing. The simulation parameters were essentially the same as those of the major species observed at X-band.

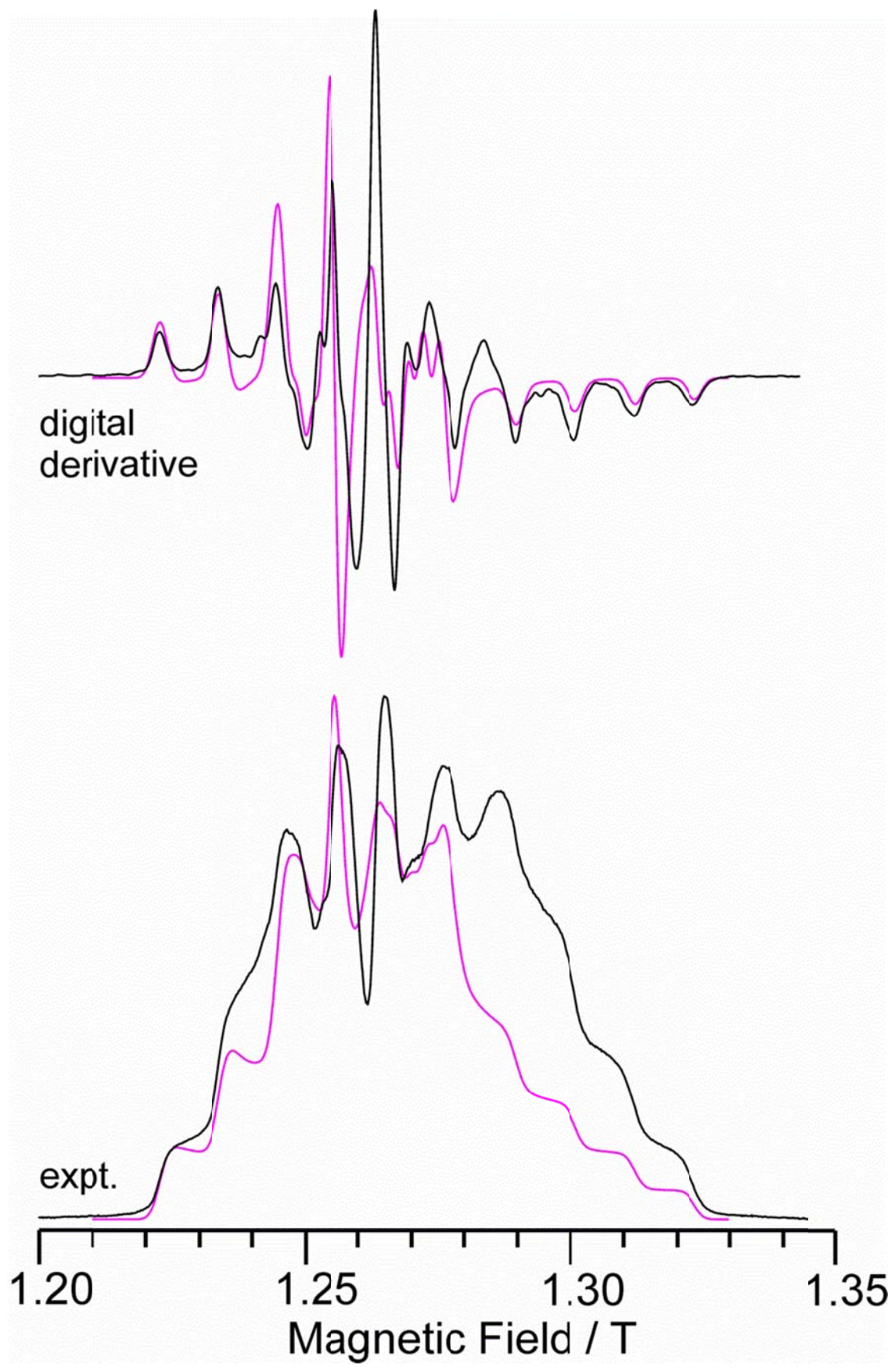




**Figure 9.** Low temperature (2 K) Q-Band EPR spectrum of **2** (0.1 mM in toluene). The lower pair of traces are the experimental spectrum (black trace), together with a simulation (magenta trace), while the upper pair is a digital derivative with a simulation. Experimental conditions: microwave frequency = 35.2650 GHz, microwave power = 2 mW, field modulation = 0.5 G, time constant = 16 ms, single 120 s scan. Simulation parameters:  $\mathbf{g} = [1.995, 1.995, 1.979]$ ,  $\mathbf{A}({}^{93}\text{Nb}) = [80, 80, 310]$  MHz,  $W = 40, 40, 45$  MHz.

In keeping with the trend in stability, complex **7** gave the most problematic frozen solution EPR behavior. There are multiple species present in these samples, albeit with similar EPR parameters. It was possible only to simulate approximately one of the species (see Figure S22, Supporting Information), although it gave an average  ${}^{181}\text{Ta}$  hyperfine coupling consistent with the room temperature value (see Table 2).

The results of fluid solution and frozen solution EPR studies can be combined, as was done by Alonso *et al.*<sup>41</sup> This makes use of the fact that in the frozen solution spectra of these systems, only  $g_{\parallel}$  and  $A_{\parallel}$  can be easily determined (single-crystal studies can provide the full tensors for both  $\mathbf{g}$  and  $\mathbf{A}$ , as done by Kirmse *et al.*),<sup>42</sup> but here, for **2** and especially **7**, the  $g_{\perp}$  and  $A_{\perp}$  values are relatively uncertain. The starting point relevant equations for an axial hyperfine interaction for a  $d_{xy/x^2-y^2}$ <sup>1</sup> ground state are as follows:

$$\begin{aligned} A_{\parallel} &= -P \left[ \kappa + \frac{4}{7} + \frac{3}{7}(g_e - g_{\perp}) + (g_e - g_{\parallel}) \right], \\ A_{\perp} &= -P \left[ \kappa - \frac{2}{7} + \frac{11}{14}(g_e - g_{\perp}) \right] \end{aligned} \quad (1a, b)$$

where  $P$  is the intrinsic hyperfine coupling constant,  $P = g_e g_N \beta_e \beta_N \langle r^{-3} \rangle_{av}$ , which for free-ion  ${}^{51}\text{V}^{4+}$  equals 516 MHz,<sup>62</sup> and for free-ion  ${}^{93}\text{Nb}^{4+}$  equals 576 MHz<sup>62</sup> (the value for  ${}^{181}\text{Ta}^{4+}$  is unavailable), and  $\kappa$  is a unitless scaling factor to account crudely for covalency. Using the relationships:

$$g_{iso} = \frac{(g_{\parallel} + 2g_{\perp})}{3}, a_{iso} = \frac{(A_{\parallel} + 2A_{\perp})}{3} \quad (2a, b)$$

By substitution of Eqns 1 into Eqn 2b, and making use of Eqn 2a to substitute for  $g_{\parallel}$  and  $g_{\perp}$ , one obtains:

$$a_{iso} = -P[\kappa + (g_e - g_{iso})] \quad (3)$$

Subtraction of Eqn 3 from Eqn 1a, and substituting for  $g_{\perp}$  from Eqn 2a, gives:

$$A_{\parallel} - a_{iso} = -P \left[ \frac{4}{7} + \frac{11}{14}(g_e - g_{\parallel}) - \frac{5}{14}(g_e - g_{iso}) \right] \quad (4)$$

allowing calculation of  $P$  in the system of interest; Eqn 3 then yields  $|\kappa|$ , since the sign of  $a_{iso}$  is not known experimentally. This method, applied to  $[V(C_6Cl_5)_4]$ , gave  $|P| = 323$  MHz,  $|\kappa| = 0.54$ ,<sup>41</sup> and for  $[Nb(C_6Cl_5)_4]$ , gave  $|P| = 352$  MHz,  $|\kappa| = 0.99$ .<sup>46</sup> This method had not been previously applied to  $V(\text{Mes})_4$ , yet this is among the most relevant complexes to ours and that for which the best EPR data are available.<sup>42</sup> We thus find here for  $V(\text{Mes})_4$ ,  $|P| = 291.5$  MHz,  $|\kappa| = 0.617$ .<sup>63</sup> The tetra(amido) complex,  $V(\text{NEt}_2)_4$ , was reported to have  $|P| = 330$  MHz,<sup>43</sup> and substituting that value and their EPR data (see Table 2) into Eqn 3 gives  $|\kappa| = 0.50$ . The tetra(alkoxido) complex,  $V(\text{O}^t\text{Bu})_4$ , had  $|P| = 324$  MHz giving  $|\kappa| = 0.55$ .<sup>44</sup> Concerning the ketimides, we calculate here for **1**,  $|P| = 207$  MHz,  $|\kappa| = 0.59$ ; and for **2**,  $|P| = 194$  MHz,  $|\kappa| = 0.94$ .<sup>64</sup> If one takes the ratio of the calculated  $P$  value to the free-ion  $P$  value, then the tetra(aryl), amido, and alkoxido vanadium(IV) complexes all give values of  $\sim 0.6$ , while the V and Nb ketimides give this ratio as roughly 0.4, indicating the much higher covalency in the latter complexes.

**UV-vis Spectroscopy.** Both complexes **1** and **2** exhibit rich UV-vis spectra (Figure 10). For example, the electronic absorption spectrum of **1** features two intense absorptions at 360 ( $\epsilon = 12000 \text{ M}^{-1}\cdot\text{cm}^{-1}$ ) and 460 nm ( $\epsilon = 6000 \text{ M}^{-1}\cdot\text{cm}^{-1}$ ), which are both assignable to ligand to metal charge transfer processes, i.e., crudely represented by  $[\text{M}^{\text{IV}}(\text{N}^{\ominus}=\text{C}^{\text{t}}\text{Bu}_2)] \rightarrow [\text{M}^{\text{III}}(\text{N}^{\bullet}=\text{C}^{\text{t}}\text{Bu}_2)]$ . Additionally, two absorptions are observed at 620 nm ( $\epsilon = 560 \text{ M}^{-1}\cdot\text{cm}^{-1}$ ) and 764 nm ( $\epsilon = 440 \text{ M}^{-1}\cdot\text{cm}^{-1}$ ). We have tentatively assigned these less intense bands to d-d transitions, as will be discussed in detail below. The UV-vis spectrum of **2** features an intense absorption at 320 nm ( $\epsilon = 12000 \text{ M}^{-1}\cdot\text{cm}^{-1}$ ), which is likewise assignable to ligand to a metal charge transfer. In addition, this spectrum features four transitions at 432 ( $\epsilon = 2700 \text{ M}^{-1}\cdot\text{cm}^{-1}$ ), 596 ( $\epsilon = 1200 \text{ M}^{-1}\cdot\text{cm}^{-1}$ ), 698 ( $\epsilon = 1400 \text{ M}^{-1}\cdot\text{cm}^{-1}$ ), and 830 nm ( $\epsilon = 1800 \text{ M}^{-1}\cdot\text{cm}^{-1}$ ), which are assignable to d-d transitions. Unfortunately, it was not possible to prepare UV-vis samples of **7** that were free of other optically absorbing components.

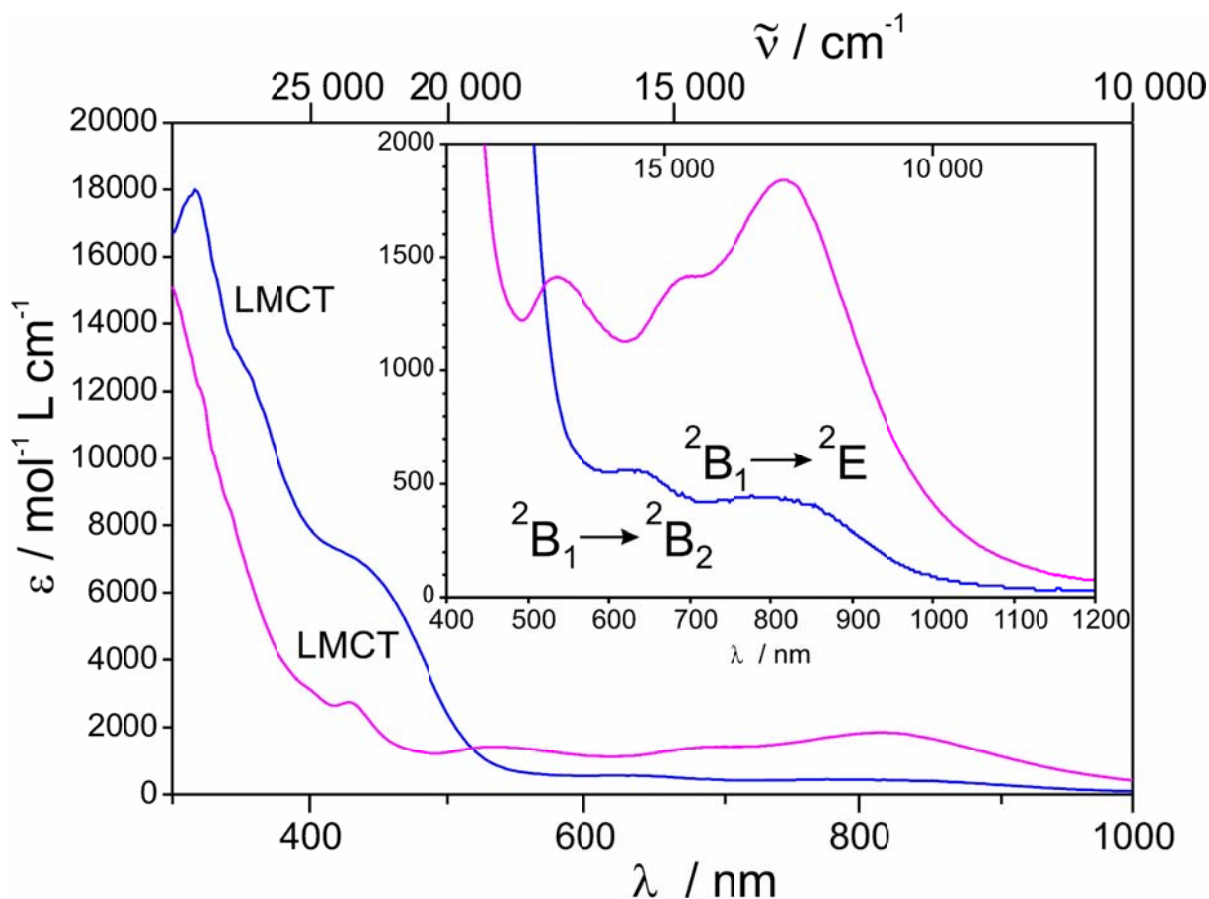


**Figure 10.** Room temperature UV-Vis-NIR absorption spectra of **1** (blue traces) and **2** (magenta traces) in hexanes solution. For both compounds, the bands in the approximate range 300 – 450 nm are due to ligand-to-metal charge transfer (LMCT) transitions. The inset shows an expansion of the Vis-NIR region with d-d band assignments as described in the text.

**Ligand Field Theory Analysis.** To employ a simple ligand-field theory for the  $[M(N=C^tBu_2)_4]$  complexes, we need to establish a physical model. In  $D_{2d}$  point group symmetry, the  $d_{x^2-y^2}$  AO is represented by  $B_1$  and its parentage (via ascent in symmetry) is  $E$  (together with  $d_{z^2}$ ) in  $T_d$ . The  $d_{xy}$  orbital is represented by  $B_2$  and its parentage (along with  $d_{xz}$  and  $d_{yz}$ ) is  $T_2$  in  $T_d$ . This symmetry and coordinate system is identical to that used by some of us in our previous study of  $[Co(N=C^tBu_2)_4]$ .<sup>6</sup> To achieve this description, we define the  $x$  and  $y$  axes as lying between the M-L bonds (bisecting the L-M-L angles) (Figure 11), which is in any case more appropriate for

an axial ( $x = y$ ) system. If the  $x$  and  $y$  axes were defined along the M-L bonds, as done by Soriaga et al.,<sup>9</sup> then the representation of  $d_{x^2-y^2}$  and  $d_{xy}$  would be reversed. Such a definition would be appropriate for  $C_{2v}$  symmetry, where  $x$  and  $y$  are symmetry inequivalent. Given the axial nature of the EPR spectra and a desire for the simplest useful model to describe  $[M(N=C^t\text{Bu}_2)_4]$  complexes, we shall use primarily  $D_{2d}$  symmetry in our simple ligand-field model.

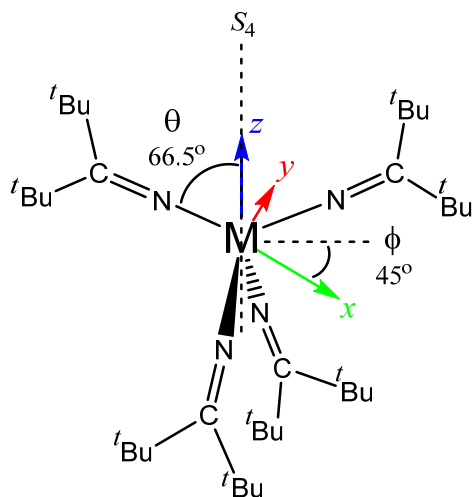


**Figure 11.** Structure of generic  $M(N=C^t\text{Bu}_2)_4$  complex showing coordinate system used for the AOM analysis. Two ketimide ligands are in the plane of the paper; one projects from the paper and the other is behind. The  $z$  axis (shown in blue) corresponds to the approximate  $S_4$  axis; the  $x$  (green) and  $y$  (red) axes are rotated  $45^\circ$  from the ligands planes. For the AOM analysis, average  $\theta$ ,  $\theta'$  values are used (ideal  $\theta = 54.7356^\circ$ ), with an ideal  $S_4$  axis ( $\phi = 45^\circ$  (as shown),  $135^\circ$ ,  $225^\circ$ ,  $315^\circ$ ). For  $M = \text{Ti}$ ,  $\theta = 56.53^\circ$ ; for  $M = \text{V}$  (**1**),  $\theta = 66.5^\circ$  (as shown); for  $M = \text{Nb}$  (**2**),  $\theta = 64.4^\circ$ ; for  $M = \text{Ta}$  (**7**),  $\theta = 64.16^\circ$ ; the angle to the other pair of ligands,  $\theta' \equiv 180^\circ - \theta$ .

We can now begin to describe the ketimide MOs involved in bonding using the angular overlap model (AOM) with an ideal  $S_4$  axis defining  $z$ , and the  $x$  and  $y$  axes between the bonds, as described above (see Figure 11). The angle  $\theta$  is given by the relevant crystal structures. This geometrical model is sufficient for the simple nature of our analysis. Soriaga *et al.* did not mention  $\sigma$ -bonding in this class of complexes,<sup>9</sup> but we note that the ketimide ligand is likely a strong  $\sigma$ -donor and this interaction alone could potentially lead to a large (for  $T_d$   $ML_4$ ) splitting,

$\Delta_{\text{tet}} = \frac{4}{3} \varepsilon_{\sigma}$ , between the  $e(d_{z^2}, d_{x^2-y^2})$  and  $t_2(d_{xz}, d_{yz}, d_{xy})$  metal ion orbitals. For illustrative purposes, we begin with only  $\sigma$ -bonding and the structure of the Ti(IV) congener, which has  $\theta$  only  $\sim 2^\circ$  away from ideal tetrahedral ( $\tau = 0.96$ ).<sup>19</sup> We can moderately well fit the two observed putative d-d electronic transitions for **1** using this nearly tetrahedral model with  $\varepsilon_{\sigma} = 10\,610\text{ cm}^{-1}$ . The ground state is  ${}^2B_1(d_{x^2-y^2})$  with the  ${}^2A_1(d_{z^2})$  excited state barely higher in energy ( $\sim 100\text{ cm}^{-1}$ ). The transition,  ${}^2B_1 \rightarrow {}^2A_1$  is forbidden in  $D_{2d}$  point group symmetry,<sup>65</sup> but the  ${}^2B_1 \rightarrow {}^2E(d_{xz, yz})$  transition is allowed with  $xy$  polarization.<sup>66</sup> It is calculated to occur at  $13\,470\text{ cm}^{-1}$ , reasonably close to experiment ( $12\,800\text{ cm}^{-1}$ , based on the band centers on an energy scale). For comparison,  $\text{VCl}_4$  has  $\Delta_{\text{tet}} = 7900\text{ cm}^{-1}$ ,<sup>67</sup> and  $\text{V}(\text{Mes})_4$  has  $\Delta_{\text{tet}} = 13\,370\text{ cm}^{-1}$ ,<sup>30</sup> giving  $\varepsilon_{\sigma} = 10\,030\text{ cm}^{-1}$ . The higher energy transition is  ${}^2B_1 \rightarrow {}^2B_2(d_{xy})$ , which is calculated to occur at  $15\,410\text{ cm}^{-1}$ , also reasonably close to experiment ( $16\,000\text{ cm}^{-1}$ ). Although this transition is forbidden,<sup>68</sup> it may become partially allowed by vibronic coupling and its intensity perhaps also benefits from underlying charge transfer band(s).<sup>69</sup> Vibronic coupling would be reasonable for **1** due to the Jahn-Teller effect. Tetrahedral  $nd^1$  is a classic Jahn-Teller active system, being  $e^1 t_2^0$  – the electron analog to the hole configuration  $t_2^6 e^3$ , as exemplified by octahedral Cu(II), for which vibronic coupling of an  $e_g$  mode ( $\nu_2$ ) provides a mechanism for Jahn-Teller distortion.<sup>70</sup>  $\text{V}(\text{Mes})_4$  and  $\text{VCl}_4$  are complexes with respectively, only  $\sigma$ -bonding and cylindrical  $\pi$ -bonding, which makes them better candidates for this effect than ketimides with their unsymmetrical  $\pi$ -bonding (i.e., making the distortion a pseudo Jahn-Teller effect). Although a (true) Jahn-Teller effect was not invoked to justify the  $D_{2d}$  symmetry of  $\text{V}(\text{Mes})_4$  (this complex

may have significant steric effects),<sup>30</sup> VCl<sub>4</sub> may exhibit this effect,<sup>67</sup> and it may be related to the observation of a nominally forbidden band in **1**.

However, a problem arises when we use the actual geometry of **1** (Figure 11). In this case, the greater distortion from tetrahedral geometry makes it impossible to fit both electronic transitions simultaneously. Either the lower or the higher band can be fit exactly using the <sup>2</sup>B<sub>1</sub> → <sup>2</sup>E assignment (with  $\epsilon_{\sigma}$  = 16 000 cm<sup>-1</sup> or  $\epsilon_{\sigma}$  = 20 000 cm<sup>-1</sup>, respectively), but not both – unless the symmetry is lowered, such that the four ketimide ligands are divided into two pairs; two with the lower  $\epsilon_{\sigma}$  value and two with the higher. This C<sub>2v</sub> split is large but not inconceivable.<sup>71</sup> The problem is not so much symmetry, but that these  $\epsilon_{\sigma}$  values are *extremely* high.<sup>72,73</sup> Thus, a model with only  $\sigma$ -bonding is unsatisfying.

Clearly,  $\pi$ -bonding must be considered, as was the case with the more electron rich Co(IV) congener.<sup>6</sup> Soriaga *et al.* identified the ketimide MOs having  $\pi$ -interactions with an electron poor metal ion.<sup>9</sup> These are shown in Figure 12, which is inspired by their work and is also a cartoon version of the more recent DFT results depicted in Figure 2 of Lewis *et al.*<sup>6</sup> The occupied,  $\pi$ -donor MO that interacts strongly with  $d_{z^2}$  (and not at all with  $d_{x^2-y^2}$  in ideal tetrahedral geometry) is labeled  $\pi$ -c,<sup>72</sup> with interaction parameterized by  $\epsilon_{\pi-c}$ , increasing the energy of  $d_{z^2}$ . The unoccupied,  $\pi$ -acceptor MO that interacts with  $d_{x^2-y^2}$  (and not at all with  $d_{z^2}$  in ideal tetrahedral geometry) is labeled  $\pi$ -s, with interaction parameterized by  $\epsilon_{\pi-s}$ , decreasing the energy of  $d_{x^2-y^2}$ . The  $d_{xz}$ ,  $d_{yz}$  AOs are moderately affected by these  $\pi$ -bonding interactions

using the AOM (see Table S2 in Supporting Information), but in V(IV) (and Cr(IV)), these empty AOs are relatively unimportant compared to their role in Co(IV).<sup>6</sup>

We also note that the electronic absorption spectra of the homoleptic V(IV) complex with  $\pi$ -donor ligands, namely, V(NEt<sub>2</sub>)<sub>4</sub>, has been recorded, both as a pure solid and in a Ti(NEt<sub>2</sub>)<sub>4</sub> host.<sup>43,74</sup> These spectra gave shoulders at 17 300 cm<sup>-1</sup> (17 065 cm<sup>-1</sup> in the Ti(IV) host) and 13 000 cm<sup>-1</sup> (13 120 cm<sup>-1</sup> in Ti(IV)), which are quite close to those absorptions observed for **1**, but they were assigned oppositely, i.e., as <sup>2</sup>B<sub>1</sub> → <sup>2</sup>E, and <sup>2</sup>B<sub>1</sub> → <sup>2</sup>B<sub>2</sub>, respectively. However, the authors were not adamant in this assignment as opposed to the reverse. These workers did not have a crystal structure; however, many years later, the structure of V(NMe<sub>2</sub>)<sub>4</sub> was reported and its geometry is much closer to tetrahedral symmetry (although still *D*<sub>2d</sub>) than the geometry of the present Group 5 ketimide complexes.<sup>24</sup> The application of modern computational methods, unavailable at the time of the EPR studies on tetra(amido) and (alkoxido) V(IV) complexes,<sup>43,44</sup> is therefore of interest, but must be the subject of future investigations.



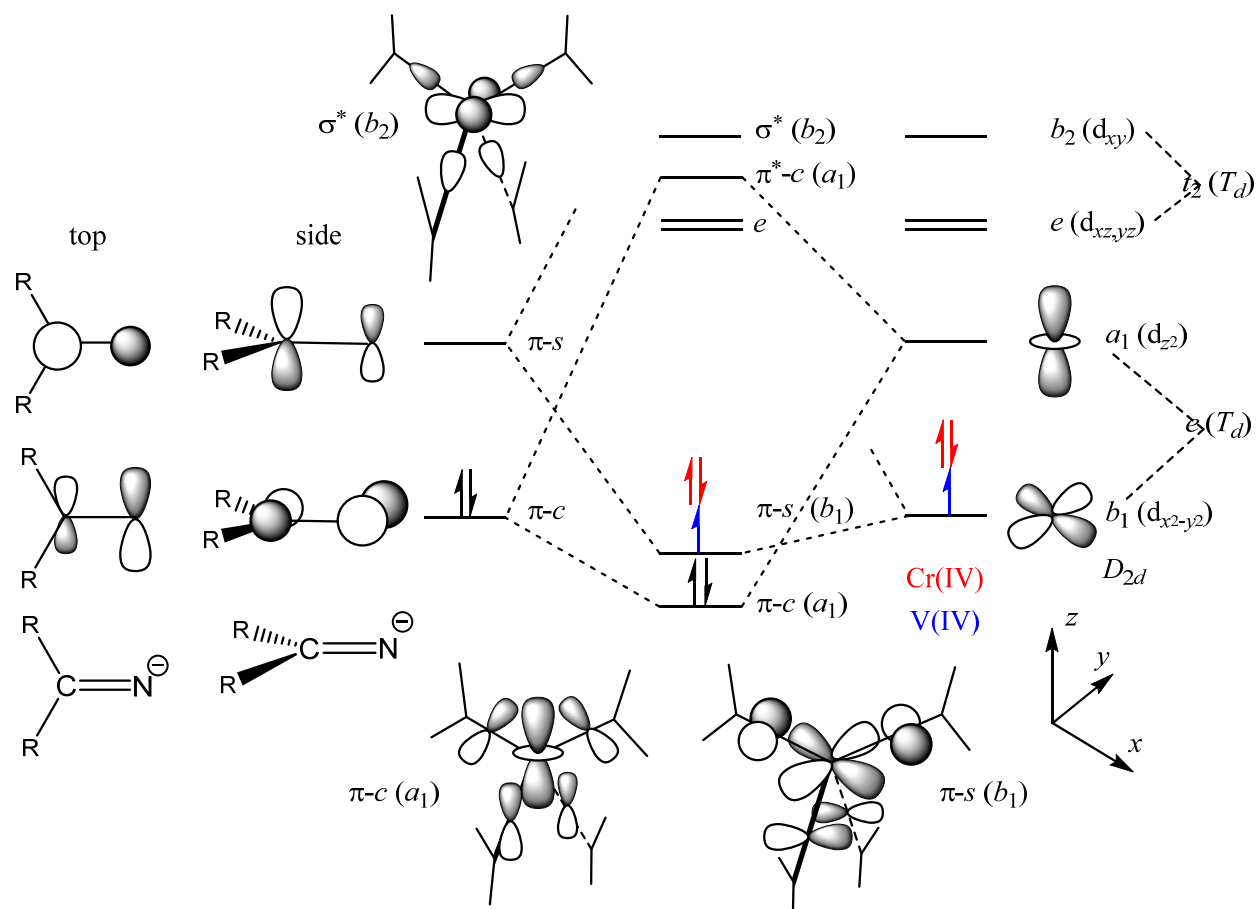


**Figure 12.** Qualitative MO diagram for V(IV) ( $d^1$ , blue electron) and Cr(IV) ( $d^2$ , red electrons) tetrakis(ketimide) complexes. On the far left are shown two views of the relevant ketimide  $\pi$ -MOs; on the far right are shown the most important metal 3d AOs, with their representations in  $T_d$  and  $D_{2d}$  symmetry. In the center is shown qualitatively the MOs resulting from interactions between the relevant ligand and metal orbitals, with representations in  $D_{2d}$  symmetry; quantitative results for V(IV) are shown in Figure 13. At the bottom are shown two of these resulting ketimide-metal MOs; for clarity, only the nitrogen  $p$  AO of the ketimide  $\pi$ -MO is shown in these diagrams. For completeness, at the top, the  $\sigma^*(b_2)$  MO is also shown, but interactions involving the unfilled  $d_{xz}$ ,  $d_{yz}$  AOs are not shown.

With this  $\pi$ -bonding model, the fit results are completely different. With three parameters  $\mathcal{E}_\sigma, \mathcal{E}_{\pi-s}, \mathcal{E}_{\pi-c}$ , it is possible to fit the two transitions exactly. The difference from the above mentioned  $\sigma$ -only analysis; however, is that while the transition at  $12\,800\text{ cm}^{-1}$  is still assigned to (allowed)  ${}^2B_1 \rightarrow {}^2E$ , and that at  $16\,000\text{ cm}^{-1}$  to (vibronically allowed)  ${}^2B_1 \rightarrow {}^2B_2$ , the forbidden

${}^2B_1 \rightarrow {}^2A_1$  transition is now calculated to occur at  $14\,800\text{ cm}^{-1}$ . This is fully possible as it would lie under existing bands. The fit parameters are:  $\mathcal{E}_\sigma = 3410\text{ cm}^{-1}$ ,  $\mathcal{E}_{\pi-c} = 4780\text{ cm}^{-1}$ , and  $\mathcal{E}_{\pi-s} = -1840\text{ cm}^{-1}$ , so that the ketimide ligands could be considered as moderate  $\sigma$ -donors, strong  $\pi$ -donors, and strong  $\pi$ -acceptors. These ketimide bonding parameters can be put into the context of other ligands of interest, although such comparison data are relatively scarce. To our knowledge, these data are not available for the amide,  $[NR_2]^-$ , ligand, which is probably the most relevant comparison for this study. However, they are known for classical neutral N-donor ligands, such as  $NH_3$ ,  $RNH_2$  (as in ethylenediamine), and  $RR'NH$  (as in 1,4,8,11-tetraazacyclotetradecane (cyclam)) when ligated to 1<sup>st</sup> row early transition metal ions such as Cr, mainly in the common 3+ oxidation state,<sup>72,73</sup> but also in higher oxidation states such as Cr(V)<sup>75</sup> and Mn(V, VI).<sup>76</sup> Briefly, these  $\sigma$ -only donors exhibit  $\mathcal{E}_\sigma \approx 7000\text{ cm}^{-1}$  (higher for the highly oxidized ions). Imine nitrogens donors come in many forms, but can be good  $\sigma$ -donors with  $\pi$ -acceptor (or donor) ability, e.g.,  $\mathcal{E}_\sigma = 6150\text{ cm}^{-1}$ ,  $\mathcal{E}_\pi = -330\text{ cm}^{-1}$  for pyridine coordinated to Cr(III).<sup>72</sup> Pyrazole nitrogens, as found in the well-known “scorpionate” ligand (hydridotris(pyrazol-1-yl)borate,  $Tp^-$ ) give  $\mathcal{E}_\sigma = 8350\text{ cm}^{-1}$ ,  $\mathcal{E}_{\pi-s} = 1300\text{ cm}^{-1}$  ( $\mathcal{E}_{\pi-c} = 0$ ) for  $[Tp_2Cr]^+$ .<sup>77</sup> with similar parameters estimated for Mn(III) in  $[Tp_2Mn]^+$ .<sup>78</sup> The extreme among N (or likely any other) donors is nitride, which exhibits  $\mathcal{E}_\sigma = 25\,000\text{ cm}^{-1}$ ,  $\mathcal{E}_\pi = 18\,000\text{ cm}^{-1}$  for Cr(V) and Mn(V).<sup>75,76</sup> Phosphines bound to late transition metal ions, e.g., Ni(II), can be described as having  $\mathcal{E}_\pi \approx -1500\text{ cm}^{-1}$ ,<sup>79</sup> comparable to what is seen here for ketimide, and are good  $\sigma$ -donors ( $\mathcal{E}_\sigma \approx 5000\text{ cm}^{-1}$ ) but have no simultaneous  $\pi$ -donor ability. Bonding parameter characterization of ketimides bound to a wider variety of metal ions is needed, but it is clear that,

while being only moderate  $\sigma$ -donors, their combination of  $\pi$ -donor and  $\pi$ -acceptor ability makes them unusual, if not unique, among N (or P) donor ligands.

We can also calculate EPR transitions using the LFT software DDN (see SI),<sup>79</sup> which also includes the electronic spin and orbital Zeeman interaction. Thus, application of an external magnetic field ( $B_0 = 350$  mT, to correspond to X-band) and inclusion of spin-orbit coupling,  $\zeta = 175$  cm<sup>-1</sup> (70% of the free-ion value, 250 cm<sup>-1</sup>)<sup>80</sup> yields  $g_{\parallel} = 1.914$  and  $g_{\perp} = 1.974$ . These  $g$  values are more anisotropic and with lower  $g_{\text{avg}}$  than experiment, but the relation  $g_{\parallel} < g_{\perp} < 2.00$  is reproduced. This is as expected from perturbation theory,<sup>81</sup> where the  $g$  values are described by:

$$\begin{aligned} g_{\parallel} &= g_e - \frac{8\zeta}{(E_{2B_2} - E_{2B_1})}, \\ g_{\perp} &= g_e - \frac{2\zeta}{(E_{2E} - E_{2B_1})} \end{aligned} \quad (5)$$

where  $(E_{2E} - E_{2B_1}) = 12\,800$  cm<sup>-1</sup> and  $(E_{2B_2} - E_{2B_1}) = 16\,000$  cm<sup>-1</sup>, so that:  $g_{\parallel} = 1.915$ ,  $g_{\perp} = 1.975$  – exactly the same values as the LFT exact calculation. The value for  $\zeta$  could of course be reduced to improve the correspondence, e.g.,  $\zeta \approx 110$  cm<sup>-1</sup> (44% of the free-ion value) matches the experimental  $g_{\perp}$ , although  $\zeta \approx 50$  cm<sup>-1</sup> – a meaninglessly low value for V(IV) – is needed to match  $g_{\parallel}$ . As shown below, quantum calculations are much more successful at not overstating the  $g$  anisotropy in this complex.

We can apply the same model to the Nb(IV) complex, **2**. In this case, there may be rhombic splitting resolved in the visible region, with bands at 12 300 cm<sup>-1</sup>, 14 300 cm<sup>-1</sup>, 18 700 cm<sup>-1</sup>, and

an additional band at 23 400 cm<sup>-1</sup>. This is similar to a band at 21 400 cm<sup>-1</sup> observed for [V(C<sub>6</sub>Cl<sub>5</sub>)<sub>4</sub>] by Alonso et al.,<sup>41</sup> but we do not attempt to assign it as we doubt that these violet/blue absorption bands are d-d in character. We note that [V(Mes)<sub>4</sub>] exhibits several bands in this region (23 870, 21 480, 18 350 cm<sup>-1</sup>), but all were assigned to CT transitions.<sup>30</sup> In any case, using the same fit procedure, the bands match exactly (the center of the first two bands is the fit result, 13 300 cm<sup>-1</sup>).<sup>82</sup> The fit parameters for **2** are:  $\epsilon_{\sigma} = 5210$  cm<sup>-1</sup>,  $\epsilon_{\pi-c} = 4670$  cm<sup>-1</sup>, and  $\epsilon_{\pi-s} = -1700$  cm<sup>-1</sup>, so there is a stronger  $\sigma$ -bonding interaction with the larger Nb(IV) ion than with V(IV), with the  $\pi$ -bonding being roughly the same. This observation is consistent with what would be expected on going down a group in the d block.

In summary, with the ligand field analysis in hand, it is now apparent that the geometry differences observed for M(amide)<sub>4</sub> and M(ketimide)<sub>4</sub> are not due to differences in  $\sigma$ - or  $\pi$ -donor ability, which are probably similarly between the two ligand types, but are instead due to the  $\pi$ -acceptor ability of the ketimide ligand, as the amide ligand is unable to act as a  $\pi$ -acceptor.

**Quantum Chemical Theory Analysis.** Analogously to what was done previously for [Co(N=C<sup>t</sup>Bu<sub>2</sub>)<sub>4</sub>],<sup>6</sup> we have used density functional theory (DFT) to probe the series of Group 5 ketimides. In the interests of computational efficiency, complexes **1** and **2** were both truncated to M(N=CMe<sub>2</sub>)<sub>4</sub>. The program ORCA by Neese<sup>83,84</sup> was employed with the B3LYP functional and def2-TZVP basis set,<sup>85,86</sup> which are widely used for transition metal complexes.<sup>87,88</sup> Further details are given in Supporting Information including representative input/output files, Tables S3 and S4, respectively, for [V(N=CMe<sub>2</sub>)<sub>4</sub>] and [Nb(N=CMe<sub>2</sub>)<sub>4</sub>]. In the latter case our computational methodology was still effective, the only qualitatively relevant point being a greater delocalization onto the ketimide nitrogen orbitals. The key result for both the V and Nb

ketimide complexes is that the appearance of the HOMO is clearly that which we have defined above as  $d_{x^2-y^2}$ , with a  $\pi^*$  interaction with the ketimide ligands, which is consistent with the ligand field analysis. This can be seen in Figure S25, which presents side-by side the spin up ( $\alpha$ ) HOMOs for  $[\text{V}(\text{N}=\text{CMe}_2)_4]$  (MO #73) and  $[\text{Nb}(\text{N}=\text{CMe}_2)_4]$  (MO #82).

The frontier MOs for  $[\text{V}(\text{N}=\text{CMe}_2)_4]$  with predominant 3d character (MOs #73 – 76, 78) are shown in Figure 13, with their calculated energies and representations in  $D_{2d}$  symmetry. Immediately below the HOMO in energy are two degenerate  $\pi$ -bonding orbitals (MOs #71, #72) that do have significant V 3d character. Their  $\pi$ -antibonding counterpart MOs with higher d character are shown in Figure 13. Overall, the MO diagram is very similar to that determined previously for the Co(IV) congener.<sup>6</sup> The chief difference between the two cases, besides the spin quartet  $d^5$  configuration for Co(IV), is that the 3d-based MOs are overall higher in energy for V(IV), as expected from its being in Group 5 as opposed to Group 9, and the energy separation between the  $b_1$  and  $e, a_1$  MOs (i.e., the HOMO-LUMO gap) is much larger, as well ( $\sim 4$  eV for V(IV) versus  $\sim 2$  eV for Co(IV)). Nevertheless, the extreme closeness in energy among the  $e, a_1$  MOs (which are half-filled in  $[\text{Co}(\text{N}=\text{C}^t\text{Bu}_2)_4]$ ) is again found for the V(IV) complex. Although we have not specifically performed calculations for the Cr(IV) congener, it is clear from our MO diagram that this complex would have a filled  $b_1$  HOMO with the triplet excited state(s) significantly higher in energy, in agreement with earlier work.<sup>9</sup>

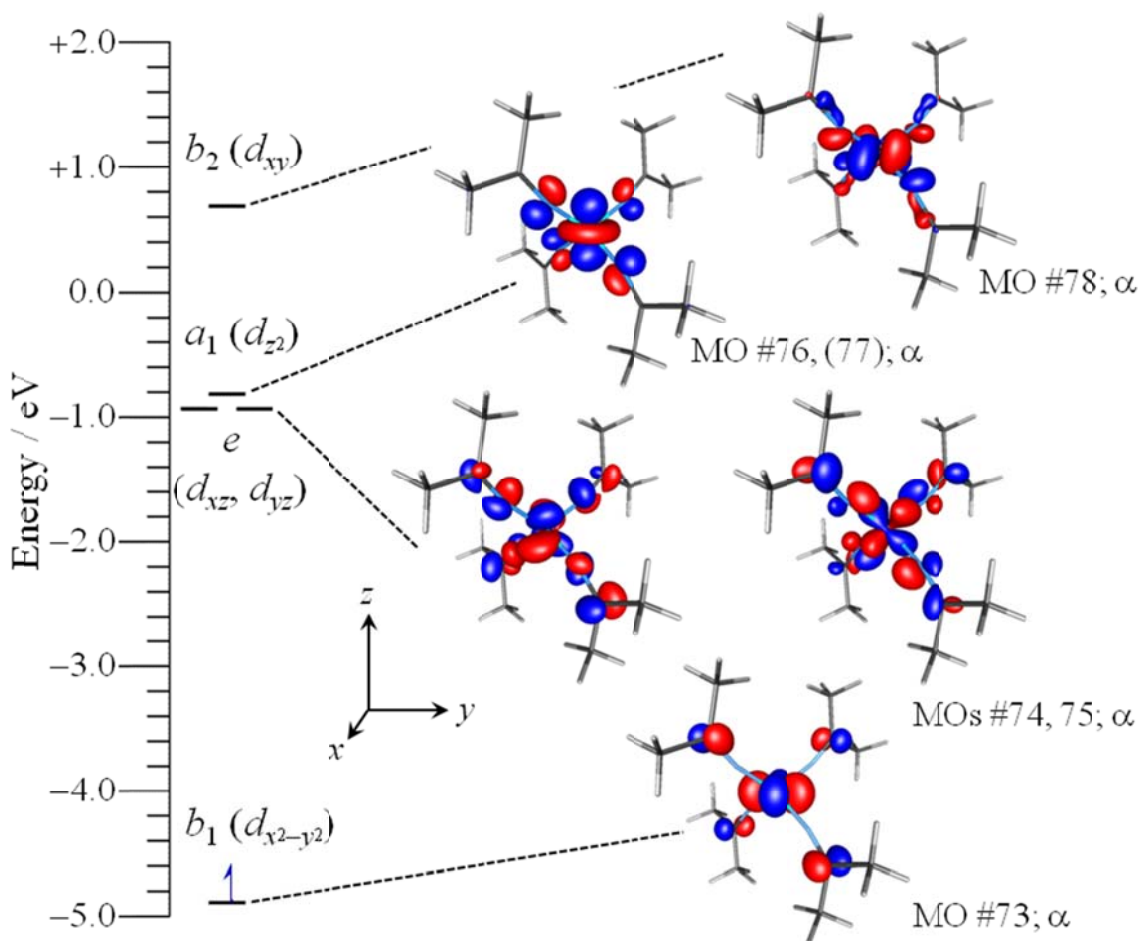


**Figure 13.** Frontier molecular orbitals for  $[V(N=CMe_2)_4]$  with representations in  $D_{2d}$  symmetry. Isosurface value = 0.06.

The corresponding MO diagram for  $[Nb(N=CMe_2)_4]$  is shown in Figure S26 (Supporting Information). The results are overall very similar to those for the V(IV) complex, with the Nb-based MOs being higher in energy. As a result, these are more in range with high-energy ligand-based MOs. Thus, there is a purely ketimide  $\pi^*$  MO (#86) lying in between two MOs each with Nb  $4d_{z^2}$  character, the latter of which (#87) appears to be a more “classical”  $4d_{z^2}$  orbital. Again, we have not performed calculations for the Mo(IV) congener, nor did Soriaga *et al.*,<sup>9</sup> but our results for  $[Nb(N=CMe_2)_4]$  give a HOMO-LUMO gap of  $\sim 3$  eV, so that the singlet ground state for  $[Mo(N=C^tBu_2)_4]$  should be greatly favored.

In addition to providing an MO picture of these Group 5 ketimide complexes, the ORCA software can calculate EPR parameters. In this case, this includes the  $\mathbf{g}$  tensor, with its orientation, and the hyperfine coupling tensors both for these magnetically active metal ions and the  $^{14}\text{N}$  atoms of the ketimide ligands. As seen in Table 3, which compares the experimental and calculated EPR parameters, the  $\mathbf{g}$  tensor anisotropy in these complexes is relatively small, making computational reproduction of the experimental data challenging. What is gratifying, however, is that for both  $[\text{V}(\text{N}=\text{CMe}_2)_4]$  and  $[\text{Nb}(\text{N}=\text{CMe}_2)_4]$  an essentially axial  $\mathbf{g}$  tensor is calculated with  $g_{\parallel} < g_{\perp} < 2.00$ . This is the result expected from simple LFT, as described above, but what is significant is that the calculated  $g$  values themselves are quite close to experiment, more so than from LFT, particularly for  $g_z$  ( $g_{\parallel}$ ,  $g_{\min}$ ), which is the best determined among the various experimental parameters. For both V and Nb complexes, the  $\mathbf{g}$  tensors derived from optimized geometries give slightly better agreement with experiment than those using the crystal structures. This may reflect the possibility that the solution structure of these complexes is less squashed than in the solid state, but the agreement may be fortuitous. Regarding the hyperfine coupling, which is an even greater computational challenge, the results are also very satisfying. In this case, the experimental values for  $A_{\perp}$  ( $^{51}\text{V}$ ,  $^{93}\text{Nb}$ ) are at best approximate, so that the agreement in  $a_{\text{iso}}$  and  $A_{\text{dip}}$  may well be better than it appears. The calculated direction of the  $\mathbf{g}$  and  $\mathbf{A}$  ( $^{51}\text{V}$ ,  $^{93}\text{Nb}$ ) tensors is as expected, with the unique (parallel) value aligned with the molecular approximate  $S_4$  axis, in agreement with LFT. As seen in Table 3, the calculations reproduce the components of the axial  $\mathbf{A}$  ( $^{51}\text{V}$ ) tensor reasonably well, noting that the only well-determined experimental value is  $A_z$  ( $A_{\parallel}$ ). Here, the results of the optimized geometry are clearly better than those from the experimental geometry, again supporting the idea that the solution structure is less squashed. However, the situation is less clear for  $\mathbf{A}$  ( $^{93}\text{Nb}$ ), where each geometry

has strengths and weaknesses in terms of matching experiment. We also note that, since **2** did not give a single species upon freezing (and **7** was even more heterogeneous), the expectations for experimental and calculated correspondence for these complexes are inherently lower.

Nevertheless, the calculated values for the  $^{14}\text{N}$  hyperfine couplings are in reasonable agreement with the experimental values (see Table 3), Even the  $^{14}\text{N}$  quadrupole couplings, of which only one component was estimated from ENDOR, are consistent between experiment and theory (Table 3). Interestingly, the calculated  $\mathbf{P}(^{14}\text{N})$  tensor was very rhombic [ $\mathbf{P}(^{14}\text{N}) = [-0.40, -1.26, +1.66]$  MHz (**1**);  $[-0.25, -1.42, +1.67]$  MHz (**2**)], which may be a consequence of the complex  $\sigma$ -donation /  $\pi$ -donation /  $\pi$ -accepting nature of the metal-ketimide interaction, as described above, leading to a very non-spherical electron distribution around the nitrogen atoms. The quadrupole coupling tensors for  $^{51}\text{V}$  and  $^{93}\text{Nb}$  were also calculated and found to be small (e.g.,  $P_{\max}(^{51}\text{V}) = -0.17$  MHz). For comparison, vanadyl complexes such as VO(salen) and VO(OEP) gave  $P_{\max}(^{51}\text{V}) = -0.29$  MHz.<sup>58,59</sup> One might expect a larger quadrupole in heteroleptic vanadyl complexes than in homoleptic **1**, but such generalization are speculative given the paucity of such data. Overall, the calculated spin Hamiltonian parameters for **1** and **2** are fully consistent with experiment, especially given the deficiencies in experimental data and in computational modeling.

**Table 3.** Experimental and Calculated  $g$  Values and Metal ( $^{51}\text{V}$ ,  $^{93}\text{Nb}$ ) and Ligand ( $^{14}\text{N}$ ) Hyperfine Coupling Constants (in MHz) for Group 5 Ketimides<sup>a</sup>

| Complex   |       | $g_{\text{iso}}$<br>(fluid), | $g_z,$<br>$g_x, g_y$<br>(frozen) <sup>f</sup> | $a_{\text{iso}}$<br>(fluid),              |                 | $A_z, A_x, A_y$<br>(frozen) <sup>e</sup> | $A_{\text{dip}}$<br>(z, x, y) <sup>f</sup> |
|---|-------|------------------------------|---|---|-----------------|--|--|
|   |       | $g_{\text{avg}}$<br>(frozen) |   | $A_{\text{avg}}$<br>(frozen) <sup>d</sup> | isotope         |  |  |
|   |       |                              |   | $^{51}\text{V} /$<br>$^{93}\text{Nb}$     | $^{14}\text{N}$ | $^{51}\text{V} / ^{93}\text{Nb}$         | $^{51}\text{V} / ^{93}\text{Nb}$           |
| [V(N=C <sup>t</sup> Bu <sub>2</sub> ) <sub>4</sub> ],<br><b>1</b> | expt. | 1.9885,<br>1.983             | 1.979,<br>1.985,                              | 124,<br>125                               | 10.5,           | 245, 65, 65                              | ∓ 120,<br>±60, ±60                         |



|  |                  |                  |                              |             |       |                           |                         |
|--|------------------|------------------|------------------------------|-------------|-------|---------------------------|-------------------------|
|  |                  |                  | 1.985                        |             |       |                           |                         |
| [V(N=CMe <sub>2</sub> ) <sub>4</sub> ]                             | XRD <sup>b</sup> | 1.9852           | 1.9824,<br>1.9866,<br>1.9864 | -85.0       | -12.8 | -214.7,<br>-19.8, -20.8   | -129.7,<br>+64.1, +65.6 |
|  | DFT <sup>c</sup> | 1.9854           | 1.9756,<br>1.9903,<br>1.9903 | -114.2      | -11.5 | -255.4,<br>-43.3, -43.8   | -141.2,<br>+70.8, +70.4 |
| [Nb(N=C <sup>t</sup> Bu <sub>2</sub> ) <sub>4</sub> ],<br><b>2</b> | expt.            | 1.9840,<br>1.988 | 1.966,<br>1.999,<br>1.999    | 185,<br>150 | ---   | 300,<br>80, 80            | ∓ 150,<br>±75, ±75      |
| [Nb(N=CMe <sub>2</sub> ) <sub>4</sub> ]                            | XRD <sup>b</sup> | 1.9803           | 1.9741,<br>1.9841,<br>1.9827 | -190.3      | -8.2  | -315.0,<br>-127.9, -128.0 | -124.7,<br>+62.4, +62.3 |
|  | DFT <sup>c</sup> | 1.9803           | 1.9646,<br>1.9882,<br>1.9882 | -203.8      | -8.4  | -340.1,<br>-135.6, -135.6 | -136.4,<br>+68.2, +68.2 |

<sup>a</sup> No sign information of hyperfine coupling constants is available experimentally.

<sup>b</sup> XRD = DFT calculation using X-ray diffraction (experimental) structure.

<sup>c</sup> DFT = DFT calculation using DFT-optimized geometry.

<sup>d</sup> The value presented for calculated  $a_{\text{iso}}(^{14}\text{N})$  is an average of those for the four nitrogen ligands, however the maximum variation among these calculated values is < 0.05 MHz, less than experimental precision.

<sup>e</sup>  $^{14}\text{N}$  hyperfine coupling was not resolved in frozen solution EPR spectra, however, ENDOR spectroscopy recorded at a field corresponding to parallel ( $z$ ) EPR transitions provided a value for  $A_z(^{14}\text{N}) \approx 14$  MHz (**1**), 11 MHz (**2**). Quadrupole coupling was also estimated from these spectra:  $P_z(^{14}\text{N}) = 0.75$  MHz (**1**), 1.0 MHz (**2**). The maximum calculated quadrupole coupling was  $P_{\text{max}}(^{14}\text{N}) = 1.7$  MHz, with a very rhombic tensor ( $\eta = \frac{|P_{\text{mid}}| - |P_{\text{min}}|}{|P_{\text{max}}|} = 0.5$  (**1**); 0.7 (**2**)); if this

were indeed the case, then analysis of a full field-dependent set of experimental ENDOR spectra would be problematic.

<sup>f</sup> The calculated orientation of the  $\mathbf{g}$  and metal nucleus  $\mathbf{A}$  tensors is with the unique value (i.e., smallest  $g$  value, largest magnitude  $A$  value) along the molecular  $z$  axis, so that  $g_z \equiv g_{\parallel}$  and  $A_z \equiv A_{\parallel}$  and with the remaining, essentially equal components exactly in between the molecular  $x$  and  $y$  axes ( $g_x \approx g_y \equiv g_{\perp}$  and  $A_x \approx A_y \equiv A_{\perp}$ ), as defined in Scheme 4 and in agreement with LFT.

## Conclusions

In summary, we have synthesized a series of homoleptic Group 5 ketimide complexes,  $M(N=C^tBu_2)_4$  ( $M = V, Nb, Ta$ ). With their syntheses, a complete set of first row  $M((N=C^tBu_2)_4)$  complexes ( $M = Ti - Co$ ), as well as two triads, the Group 6 triad (which reported by Hoffman)<sup>9</sup> and now the Group 5 triad, have been isolated and fully characterized. In the solid state, the Group 5 ketimide complexes feature squashed tetrahedral ( $D_{2d}$ ) geometries. Both EPR spectroscopic results and DFT calculations support a  $d_{x^2-y^2}^1$  ( ${}^2B_1$  in  $D_{2d}$ ) ground state for this series of complexes. EPR spectroscopy also reveals that the M-L interaction in  $M(N=C^tBu_2)_4$  is far more covalent than the M-L interactions in the related tetra(aryl) vanadium(IV) complexes. A ligand field analysis of the vanadium and niobium congeners also supports the presence of a strongly covalent metal-ketimide interaction. Most importantly, however, this comprehensive investigation provides experimental verification that the ketimide ligand is a good  $\sigma$ -donor, strong  $\pi$ -donor, and strong  $\pi$ -acceptor, a combination that is not found amine, imine, or phosphine ligands. The combination of strong  $\pi$ -donor and  $\pi$ -acceptor ability places the ketimide ligand within a select group of organometallic ligands. For comparison, both the cyclopentadienyl anion and benzene can act as simultaneous  $\pi$ -donors and  $\delta$ -acceptors, which is a similar bonding situation to that seen for ketimide.<sup>89</sup> Although it should be noted that Cp is not considered a particularly good  $\delta$ -acceptor ligand.<sup>89,90</sup> We suggest that the combined acceptor and donor ability of the ketimide ligand should make it capable of stabilizing both high and low oxidation states at the same metal center, potentially permitting the development of unusual catalytic cycles.

**Supporting Information.** Experimental and computational details, spectral data, CIF files, and additional figures and tables. This material is available free of charge via the Internet at <http://pubs.acs.org>.

## AUTHOR INFORMATION

### Corresponding Authors

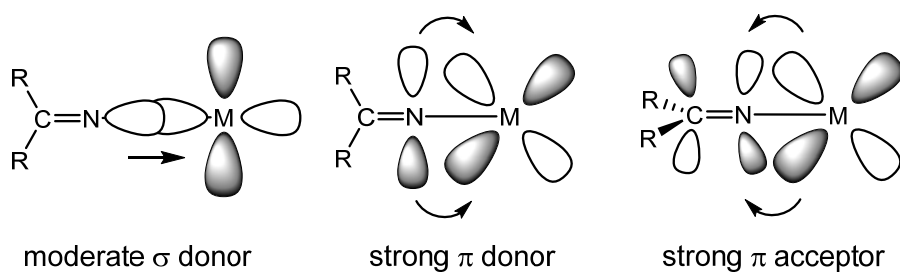
\*Email: [hayton@chem.ucsb.edu](mailto:hayton@chem.ucsb.edu), [jtelsr@roosevelt.edu](mailto:jtelsr@roosevelt.edu)

## ACKNOWLEDGMENT

We thank the National Science Foundation (CHE 1361654) for financial support of this work. We thank Prof. Brian M. Hoffman, Northwestern University, for use of the X- and Q-band EPR spectrometers in his laboratory, which is supported by the NIH (GM 111097 to B.M.H.). We also thank Prof. T. David Harris and Mr. Kang Du, Northwestern University, for use of their glove box and assistance with air-sensitive EPR sample preparation. We thank Dr. Andrew Ozarowski, National High Magnetic Field Laboratory, for providing the program CRYSTAL and assisting with its use. We thank Prof. Jesper Bendix, Copenhagen University, for providing the program Ligfield and helpful comments. Finally, we thank Dr. Guang Wu, University of California Santa Barbara, for assistance in collecting X-ray crystallographic data, and Anthony DeMartino for preliminary investigations in this area.

## TOC Graphic

### Ketimide Bonding Characteristics:



**TOC Synopsis:** A ligand field analysis of the  $d^1$  ketimide complexes  $M(N=C^tBu_2)_4$  ( $M = V, Nb, Ta$ ) reveals that the ketimide ligand is a good  $\sigma$ -donor, strong  $\pi$ -donor, and strong  $\pi$ -acceptor. The combination of strong  $\pi$ -donor and  $\pi$ -acceptor ability places the ketimide ligand within a select group of organometallic ligands.

## References

- (1) Kiplinger, J. L.; Morris, D. E.; Scott, B. L.; Burns, C. J. *Organometallics* **2002**, *21*, 3073-3075.
- (2) Graves, C. R.; Vaughn, A. E.; Schelter, E. J.; Scott, B. L.; Thompson, J. D.; Morris, D. E.; Kiplinger, J. L. *Inorg. Chem.* **2008**, *47*, 11879-11891.
- (3) Lewis, R. A.; Wu, G.; Hayton, T. W. *J. Am. Chem. Soc.* **2010**, *132*, 12814-12816.
- (4) Lewis, R. A.; Wu, G.; Hayton, T. W. *Inorg. Chem.* **2011**, *50*, 4660-4668.
- (5) Seaman, L. A.; Wu, G.; Edelstein, N.; Lukens, W. W.; Magnani, N.; Hayton, T. W. *J. Am. Chem. Soc.* **2012**, *134*, 4931-4940.
- (6) Lewis, R. A.; George, S. P.; Chapovetsky, A.; Wu, G.; Figueroa, J. S.; Hayton, T. W. *Chem. Commun.* **2013**, *49*, 2888-2890.
- (7) Lewis, R. A.; Smiles, D. E.; Darmon, J. M.; Stieber, S. C. E.; Wu, G.; Hayton, T. W. *Inorg. Chem.* **2013**, *52*, 8218-8227.
- (8) Cotton, F. A.; Wilkinson, G.; Murillo, C. A.; Bochmann, M. *Advanced Inorganic Chemistry*; 6th ed.; John Wiley & Sons, Inc.: New York, 1999.
- (9) Soriaga, R. A. D.; Nguyen, J. M.; Albright, T. A.; Hoffman, D. M. *J. Am. Chem. Soc.* **2010**, *132*, 18014-18016.
- (10) Manzer, L. E. *Inorg. Chem.* **1977**, *16*, 525-528.
- (11) Deutscher, R. L.; Kepert, D. L. *Inorg. Chem.* **1970**, *9*, 2305-2310.
- (12) Schäfer, H.; Kahlenberg, F. *Z. Anorg. Allg. Chem.* **1960**, *305*, 178-189.
- (13) Arteaga-Müller, R.; Tsurugi, H.; Saito, T.; Yanagawa, M.; Oda, S.; Mashima, K. *J. Am. Chem. Soc.* **2009**, *131*, 5370-5371.
- (14) Marchetti, F.; Pampaloni, G.; Zacchini, S. *Dalton Trans.* **2008**, 7026-7035.
- (15) Marchetti, F.; Pampaloni, G.; Zacchini, S. *Inorg. Chem.* **2007**, *47*, 365-372.
- (16) Casanova, D.; Alemany, P.; Bofill, J. M.; Alvarez, S. *Chem. Eur. J.* **2003**, *9*, 1281-1295.
- (17) Mashima, K.; Tanaka, Y.; Nakamura, A. *Organometallics* **1995**, *14*, 5642-5651.
- (18) Strauch, H. C.; Erker, G.; Fröhlich, R. *Organometallics* **1998**, *17*, 5746-5757.
- (19) Martins, A. M.; Marques, M. M.; Ascenso, J. R.; Dias, A. R.; Duarte, M. T.; Fernandes, A. C.; Fernandes, S.; Ferreira, M. J.; Matos, I.; Conceição Oliveira, M.; Rodrigues, S. S.; Wilson, C. J. *Organomet. Chem.* **2005**, *690*, 874-884.
- (20) Heinselman, K. S.; Miskowski, V. M.; Geib, S. J.; Wang, L. C.; Hopkins, M. D. *Inorg. Chem.* **1997**, *36*, 5530-5538.
- (21) Marchetti, F.; Pampaloni, G.; Zacchini, S. *Dalton Trans.* **2007**, 4343-4351.
- (22) Marchetti, F.; Pampaloni, G.; Zacchini, S. *Eur. J. Inorg. Chem.* **2008**, 2008, 453-462.
- (23) Yang, L.; Powell, D. R.; Houser, R. P. *Dalton Trans.* **2007**, 955-964.
- (24) Dubberley, S. R.; Tyrrell, B. R.; Mountford, P. *Acta Crystallogr. C.* **2001**, *57*, 902-904.
- (25) Yamada, J.; Fujiki, M.; Nomura, K. *Organometallics* **2005**, *24*, 2248-2250.
- (26) Zhang, W.; Nomura, K. *Inorg. Chem.* **2008**, *47*, 6482-6492.
- (27) Yamada, J.; Fujiki, M.; Nomura, K. *Organometallics* **2007**, *26*, 2579-2588.
- (28) Onishi, Y.; Katao, S.; Fujiki, M.; Nomura, K. *Organometallics* **2008**, *27*, 2590-2596.
- (29) Zhang, W.; Yamada, J.; Nomura, K. *Organometallics* **2008**, *27*, 5353-5360.

- (30) Głowiak, T.; Grobelny, R.; Jeżowska-Trzeblatowska, B.; Kreisel, G.; Seidel, W.; Uhlig, E. *J. Organomet. Chem.* **1978**, *155*, 39-46.
- (31) Bott, S. G.; Hoffman, D. M.; Rangarajan, S. P. *Inorg. Chem.* **1995**, *34*, 4305-4310.
- (32) Perera, T. H.; Lord, R. L.; Heeg, M. J.; Schlegel, H. B.; Winter, C. H. *Organometallics* **2012**, *31*, 5971-5974.
- (33) Mashima, K.; Matsuo, Y.; Tani, K. *Organometallics* **1999**, *18*, 1471-1481.
- (34) Krishnamurthy, R.; Schaap, W. B. *J. Chem. Educ.* **1969**, *46*, 799-null.
- (35) Suh, S.; Hoffman, D. M. *Inorg. Chem.* **1996**, *35*, 5015-5018.
- (36) Lehn, J.-S. M.; van der Heide, P.; Wang, Y.; Suh, S.; Hoffman, D. M. *J. Mater. Chem.* **2004**, *14*, 3239-3245.
- (37) Wilson, R.; Kivelson, D. *The Journal of Chemical Physics* **1966**, *44*, 154-168.
- (38) Labauze, G.; Samuel, E.; Livage, J. *Inorg. Chem.* **1980**, *19*, 1384-1386.
- (39) Muller, E. G.; Petersen, J. L.; Dahl, L. F. *J. Organomet. Chem.* **1976**, *111*, 91-112.
- (40) Muller, E. G.; Watkins, S. F.; Dahl, L. F. *J. Organomet. Chem.* **1976**, *111*, 73-89.
- (41) Alonso, P. J.; Forniés, J.; García-Monforte, M. A.; Martín, A.; Menjón, B. *Chem. Eur. J.* **2005**, *11*, 4713-4724.
- (42) Kirmse, R.; Stach, J.; Kreisel, G. *J. Organomet. Chem.* **1981**, *210*, 73-82.
- (43) Holloway, C. E.; Mabbs, F. E.; Smail, W. R. *Journal of the Chemical Society A: Inorganic, Physical, Theoretical* **1968**, 2980-2984.
- (44) Kokoszka, G. F.; Allen Jr., H. C.; Gordon, G. *Inorg. Chem.* **1966**, *5*, 91-93.
- (45) Froncisz, W.; Hyde, J. S. *J. Chem. Phys.* **1980**, *73*, 3123-3131.
- (46) Alonso, P. J.; Ara, I.; Arauzo, A. B.; García-Monforte, M. A.; Menjón, B.; Rillo, C. *Angew. Chem. Int. Ed.* **2010**, *49*, 6143-6146.
- (47) Bigmore, H. R.; Zuideveld, M. A.; Kowalczyk, R. M.; Cowley, A. R.; Kranenburg, M.; McInnes, E. J. L.; Mountford, P. *Inorg. Chem.* **2006**, *45*, 6411-6423.
- (48) Green, J. C.; Green, M. L. H.; Kaltsoyannis, N.; Mountford, P.; Scott, P.; Simpson, S. J. *Organometallics* **1992**, *11*, 3353-3361.
- (49) Noh, W.; Girolami, G. S. *Inorg. Chem.* **2008**, *47*, 535-542.
- (50) Munhá, R. F.; Zarkesh, R. A.; Heyduk, A. F. *Inorg. Chem.* **2013**, *52*, 11244-11255.
- (51) Nguyen, A. I.; Blackmore, K. J.; Carter, S. M.; Zarkesh, R. A.; Heyduk, A. F. *J. Am. Chem. Soc.* **2009**, *131*, 3307-3316.
- (52) Petersen, J. L.; Griffith, L. *Inorg. Chem.* **1980**, *19*, 1852-1858.
- (53) Mailer, C.; Taylor, C. P. S. *Biochim. Biophys. Acta* **1973**, *322*, 195-203.
- (54) Baute, D.; Goldfarb, D. *J. Phys. Chem. A* **2005**, *109*, 7865-7871.
- (55) Mustafi, D.; Galtseva, E. V.; Krzystek, J.; Brunel, L.-C.; Makinen, M. W. *J. Phys. Chem. A* **1999**, *103*, 11279-11286.
- (56) Kirste, B.; Van Willigen, H. *The Journal of Physical Chemistry* **1982**, *86*, 2743-2749.
- (57) Mulks, C. F.; Kirste, B.; Van Willigen, H. *Journal of the American Chemical Society* **1982**, *104*, 5906-5911.
- (58) Aznar, C. P.; Deligiannakis, Y.; Tolis, E. J.; Kabanos, T.; Brynda, M.; Britt, R. D. *J. Phys. Chem. A* **2004**, *108*, 4310-4321.
- (59) Grant, C. V.; Ball, J. A.; Hamstra, B. J.; Pecoraro, V. L.; Britt, R. D. *J. Phys. Chem. B* **1998**, *102*, 8145-8150.
- (60) Fallis, I. A.; Murphy, D. M.; Willock, D. J.; Tucker, R. J.; Farley, R. D.; Jenkins, R.; Strevens, R. R. *Journal of the American Chemical Society* **2004**, *126*, 15660-15661.
- (61) Mustafi, D.; Makinen, M. W. *Inorganic Chemistry* **2005**, *44*, 5580-5590.

- (62) McGarvey, B. R. *J. Phys. Chem.* **1967**, *71*, 51-66.
- (63) These values are calculated using the reported frozen solution average values for  $a_{\text{iso}}$ ,  $g_{\text{iso}}$ ; use of the fluid solution values gives:  $|P| = 318.8$  MHz,  $|\kappa| = 0.510$
- (64) For **7**,  $|P| = 152$  MHz,  $|\kappa| = 1.6$ . This value of  $|\kappa| > 1$  is not physically reasonable (i.e., a larger coupling than in the free-ion). The lack of definitive EPR low temperature data for **7** makes this analysis inapplicable compared to the V and Nb ketimides.
- (65) Even if  $C_{2v}$  symmetry is used, this transition, which becomes  ${}^2A_2 \rightarrow {}^2A_1$ , is still forbidden.
- (66) In  $T_d$  symmetry this transition directly gives  $\Delta_{\text{tet}}$ ; in  $C_{2v}$  symmetry, this would simply split into  ${}^2A_2 \rightarrow {}^2B_1$  ( $d_{xz}$ ,  $y$  allowed) and  ${}^2A_2 \rightarrow {}^2B_2$  ( $d_{yz}$ ,  $x$  allowed).
- (67) Clark, R. J. H.; Machin, D. J. *J. Chem. Soc.* **1963**, 4430-4433.
- (68) Note that if the ground state were  ${}^2A_1$ , then this transition would be allowed with  $z$  polarization. Again even if  $C_{2v}$  symmetry is used, this transition, which becomes  ${}^2A_2 \rightarrow {}^2A_1$ , is still forbidden.
- (69) Considering only the  $MN_4$  core, the nine normal vibrational modes in  $D_{2d}$  are:  $a_1$  ( $\times 2$ , IR forbidden),  $b_1$  (IR forbidden),  $b_2$  ( $\times 2$ , IR allowed), and  $e$  ( $\times 2$ , IR allowed). N.B. lower case is used for vibrations to distinguish from electronic transitions. Vibronic coupling with the  $e$  modes would make this electronic transition allowed:  $a_1 \times {}^2B_1 \times (E) \times {}^2B_2 \times (e) = A_1 + \dots$
- (70) Riley, M. J.; Hitchman, M. A.; Mohammed, A. W. *J. Chem. Phys.* **1987**, *87*, 3766-3778.
- (71) Alonso et al., in their study of in situ generated  $[V(C_6Cl_5)_4]$ , reported bands at 14 950 and 16 680  $\text{cm}^{-1}$  (there appears to be no resolution between these bands; the higher one could charitably be called a shoulder). See Ref. 41
- (72) Figgis, B. N.; Hitchman, M. A. *Ligand Field Theory and its Applications*; Wiley-VCH: New York, 2000.
- (73) Miessler, G. L.; Fischer, P. J.; Tarr, D. A. *Inorganic Chemistry*; Pearson: Upper Saddle River, NJ, 2014.
- (74) The UV-vis spectrum of the related homoleptic alkoxido complex,  $V(O^t\text{Bu})_4$ , consists of a single broad band at 13 500  $\text{cm}^{-1}$ , simply assigned to  ${}^2E \rightarrow {}^2T_2$  in  $T_d$  symmetry. See Ref. 44
- (75) Meyer, K.; Bendix, J.; Bill, E.; Weyhermüller, T.; Wieghardt, K. *Inorg. Chem.* **1998**, *37*, 5180-5188.
- (76) Meyer, K.; Bendix, J.; Metzler-Nolte, N.; Weyhermüller, T.; Wieghardt, K. *J. Am. Chem. Soc.* **1998**, *120*, 7260-7270.
- (77) Fujihara, T.; Schönherr, T.; Kaizaki, S. *Inorg. Chim. Acta* **1996**, *249*, 135-141.
- (78) Forshaw, A. P.; Smith, J. M.; Ozarowski, A.; Krzystek, J.; Smirnov, D.; Zvyagin, S. A.; Harris, T. D.; Karunadasa, H. I.; Zdrozny, J. M.; Schnegg, A.; Holldack, K.; Jackson, T. A.; Alamiri, A.; Barnes, D. M.; Telser, J. *Inorg. Chem.* **2013**, *52*, 144-159.
- (79) Desrochers, P. J.; Telser, J.; Zvyagin, S. A.; Ozarowski, A.; Krzystek, J.; Vivic, D. A. *Inorg. Chem.* **2006**, *45*, 8930-8941.
- (80) Bendix, J.; Brorson, M.; Schäffer, C. E. *Inorg. Chem.* **1993**, *32*, 2838-2849.
- (81) McGarvey, B. R. In *Transition Metal Chemistry*; Carlin, R. L., Ed.; Marcel Dekker: New York, 1966, p 89-201.
- (82) It is possible to match all of the bands exactly by dividing the ligands into pairs, but this allows for six fit parameters and is thus overparameterized.
- (83) ORCA - an *ab initio*, Density Functional and Semiempirical Program Package, 3.0.3, Neese, F., Max Planck Institut für Chemische Energiekonversion, Mülheim an der Ruhr, Germany, 2014, <https://orcaforum.cec.mpg.de/>

- (84) Neese, F. *Wiley Interdisciplinary Reviews: Computational Molecular Science* **2012**, *2*, 73-78.
- (85) Schäfer, A.; Horn, H.; Ahlrichs, R. *J. Chem. Phys.* **1992**, *97*, 2571-2577.
- (86) Weigend, F.; Ahlrichs, R. *Phys. Chem. Chem. Phys.* **2005**, *7*, 3297-3305.
- (87) Roemelt, M.; Neese, F. *J. Phys. Chem. A* **2013**, *117*, 3069-3083.
- (88) Maganas, D.; Sottini, S.; Kyritsis, P.; Groenen, E. J. J.; Neese, F. *Inorg. Chem.* **2011**, *50*, 8741-8754.
- (89) Rayón, V. M.; Frenking, G. *Organometallics* **2003**, *22*, 3304-3308.
- (90) Crabtree, R. H. *The Organometallic Chemistry of the Transition Metals*; 3rd ed.; John Wiley & Sons: New York, 2001.